Interaction Profiling Identifies the Human Nuclear EXosome Targeting (NEXT) Complex

Michal Lubas[1,2,3,#], Marianne S. Christensen[1,#], Maiken S. Kristiansen[1,#], Michal Domanski[1], Lasse G. Falkenby[4], Søren Lykke-Andersen[1], Jens S. Andersen[4], Andrzej Dziembowski[2,3,*] and Torben Heick Jensen[1,*]

[1]Centre for mRNP Biogenesis and Metabolism, Department of Molecular Biology, Aarhus University, C. F. Møllers Allé 3, Bldg. 1130, DK-8000 Aarhus C, Denmark, [2]Institute of Biochemistry and Biophysics, Polish Academy of Sciences, ul. Pawinskiego 5a, 02-106 Warsaw, Poland, [3]Department of Genetics and Biotechnology, Faculty of Biology, University of Warsaw, ul. Pawinskiego 5a, 02-106 Warsaw, Poland, [4]Department of Biochemistry and Molecular Biology, University of Southern Denmark, Odense, Campusvej 55, DK-5230 Odense, Denmark

[#] Equal contribution

*Corresponding authors: Torben Heick Jensen (thj@mb.au.dk), Andrzej Dziembowski (andrzejd@ibb.waw.pl)

Running title: human nuclear exosome activators

The RNA exosome is a conserved degradation machinery, which obtains full activity only when associated with co-factors. The most prominent activator of the yeast nuclear exosome is the RNA helicase Mtr4p, acting in the context of the Trf4p/Air2p/Mtr4p polyadenylation (TRAMP) complex. The existence of similar activator(s) in humans remains elusive. By establishing an interaction network of the human nuclear exosome, we identify the trimeric Nuclear EXosome Targeting (NEXT) complex, containing hMTR4, the Zn-knuckle protein ZCCHC8 and the putative RNA binding protein RBM7. ZCCHC8 and RBM7 are excluded from nucleoli and consistently, NEXT is specifically required for the exosomal degradation of promoter-upstream transcripts (PROMPTs). We also detect putative homologues TRAMP subunits hTRF4-2 (Trf4p) and ZCCHC7 (Air2p) in hRRP6 and hMTR4 precipitates. However, at least ZCCHC7 function is restricted to nucleoli. Our results suggest that human nuclear exosome degradation pathways comprise modules of spatially organized co-factors that diverge from the yeast model.

Introduction

Cells rely on processing and turnover pathways to control their steady-state RNA levels. In addition, the efficient elimination of malformed molecules and transcriptional by-products is constantly required, demanding a subset of robust nucleases. The major eukaryotic 3'-5' exonucleolytic activity is supplied by the multi-subunit RNA exosome complex. It resides in both cytoplasmic and nuclear compartments and participates in a wealth of reactions, including the processing of rRNA, snoRNA and snRNA, the turnover of mRNA and the surveillance of most cellular RNA species (for recent reviews see (Houseley and Tollervey, 2009; Lykke-Andersen et al., 2009)).

First discovered in the yeast *Saccharomyces cerevisiae*, the exosome consists of a catalytically inactive nine-subunit core, that obtains its ribonucleolytic activity from associated subunits. These include the nuclear/cytoplasmic and processive 3'-5' exo/endo-nuclease Dis3p/Rrp44p as well as the nuclear-specific and distributive 3'-5' exonuclease Rrp6p (Allmang et al., 1999; Mitchell et al., 1997). Although active *in vitro*, the exosome needs appropriate activators and adapters for full function *in vivo*. While activators are integral to exosome activity, adapters may rather direct the exosome to its many substrates and therefore be particular to discrete processing/degradation pathways or even recognize specific RNA features. However, as activators and adapters often co-appear in larger complexes, a clear biochemical distinction between the two is difficult to make. Central for exosome activation is an associated RNA helicase activity. In the yeast cytoplasm, this task is performed by the Ski2p DEVH ATPase in the context of the trimeric SKI complex (Anderson and Parker, 1998; Brown et al., 2000), while the DExH/D box RNA

helicase Mtr4p is an essential activator of the yeast nuclear exosome (Allmang et al., 1999; de la Cruz et al., 1998). Several Mtr4p activities are carried out in the context of the TRAMP complex, co-composed of one of the two non-canonical poly(A) polymerases, Trf4p or Trf5p, and one of the two Zn-knuckle proteins, Air1p or Air2p (LaCava et al., 2005; San Paolo et al., 2009; Wyers et al., 2005). TRAMP is suggested to target RNA, presumably through Air1p/Air2p, and trigger its processing/degradation via the 3'end-addition of an unstructured oligo(A) tail, enabling substrate unwinding by Mtr4p in preparation for exosomal nucleolysis. Interestingly, although Trf4p and Trf5p are close homologs and partially redundant (Houseley and Tollervey, 2006), Trf5p activity reportedly occurs in the yeast nucleolus, while Trf4p substrates are often non-nucleolar (Dez et al., 2007; Rougemaille et al., 2007; Wery et al., 2009; Wyers et al., 2005). Thus, exosome co-activator composition is not only different between the yeast nucleus and cytoplasm, but also inside the nucleus between the nucleolus and the remainder of the nucleoplasm. The mechanistic rationale for such division is not clear. Regardless, as a reflection of its broad nuclear localization, tRNA, sn/snoRNA, pre-rRNAs, aberrant mRNA and a class of non-coding cryptic unstable transcripts (CUTs) are all TRAMP-dependent exosome substrates (Allmang et al., 1999; Milligan et al., 2005; Reis and Campbell, 2007; van Hoof et al., 2000). In addition to TRAMP, the nuclear exosome co-operates with additional RNA binding proteins, which are currently best described as exosome/RNA adapters; (i) Rrp47p binds structured RNA substrates, associates with Rrp6p and is needed for Rrp6p-dependent exosome activities (Mitchell et al., 2003; Stead et al., 2007), (ii) Mpp6p binds poly(U) RNA, is genetically linked to Rrp47p/Rrp6p and is important for many nuclear exosome activities (Milligan et al., 2008), and (iii) the Nrd1p, Nab3p and Sen1p proteins associate with RNA

polymerase II and nascent RNA to recruit the nuclear exosome and TRAMP to process or completely degrade short transcripts, snoRNAs and CUTs, respectively (Vasiljeva and Buratowski, 2006). Moreover, the Nrd1p/Nab3p/Sen1p complex targets some RNA polymerase III transcripts, such as hypomodified, unedited or unspliced tRNAs (Wlotzka et al., 2011).

The human RNA exosome also exists in cytoplasmic and nuclear forms, that share the highly conserved nine-subunit core. However, unlike in yeast, where Dis3p is the only processive exonuclease component, two Dis3p homologs have been found to associate with the human exosome core: hDIS3 present mainly in the nucleus and hDIS3L restricted to the cytoplasm (Tomecki et al., 2010). While nuclear hDIS3 appears largely excluded from nucleoli, the third exosome-associated nuclease, hRRP6 (PM/Scl100), accumulates in nucleoli, although it can also be detected in the non-nucleolar part of the nucleoplasm and to a minor extent in the cytoplasm (Lejeune et al., 2003; Staals et al., 2010; Tomecki et al., 2010). This differential composition and localization of exosome variants is also reflected by the substrate preferences of the complex *in vivo* (Lykke-Andersen et al., 2011).

Much less is known about human exosome activators/adapters. Functional homologs of Rrp47p (C1D), Mpp6p (hMPP6) and Mtr4p (hMTR4, also called SKIV2L2) have been identified and suggested to help recruit the nuclear exosome to its substrates (Milligan et al., 2008; Schilders and Pruijn, 2008; Schilders et al., 2007; Tomecki et al., 2010). However, mechanistic detail is still lacking. Moreover, clear experimental evidence of TRAMP-like complexes outside of *S. cerevisiae* and *S. pombe* has not been obtained, despite the fact that at the sequence level this complex appears well conserved in e.g. *T. brucei* (Cristodero and Clayton, 2007; Etheridge et al., 2009) and *D. melanogaster* (Nakamura et al., 2008). Also in human

cells, candidate TRAMP components, in addition to hMTR4, are present; the closest homologs of Trf4/5p are hTRF4-1 (POLS) and hTRF4-2 (PAPD5). The latter was recently found to contribute to the 3'end adenylation of RNA polymerase I transcripts targeted by the exosome (Shcherbik et al., 2010). However, this is the only direct example of adenylation potentially being part of an RNA decay mechanism in *Metazoa*. Finally, the Zn-knuckle protein ZCCHC7 has been suggested to be a candidate Air1p/Air2p sequence homolog (Houseley and Tollervey, 2008).

Here we use co-immunoprecipitation (co-IP) analyses of human nuclear exosome complexes coupled to high resolution mass spectrometry (MS) to discover a stable trimer, which we coin the Nuclear EXosome Targeting (NEXT) complex. NEXT contains hMTR4, the putative RNA binding protein RBM7 and the Zn-knuckle protein ZCCHC8. RBM7 and ZCCHC8 are excluded from nucleoli and their depletion leads to the selective stabilization of promoter upstream transcripts (PROMPTs). We also detect hTRF4-2 and ZCCHC7 in hRRP6/hMTR4 precipitates, and consistent with their nucleolar localization, these factors impact the 3'adenylation of rRNA degradation products. Our results identify new human exosome co-factors, demonstrate their differential nuclear partitioning and show a surprising divergence from the *S. cerevisiae* system.

Results

hMTR4 association with the nuclear exosome is stabilized by hRRP6

We previously reported that three nucleolytic subunits, hRRP6, hDIS3 and hDIS3L, associate with the human core exosome (Tomecki et al., 2010). Of these, hRRP6 and hDIS3 mainly localize to the nucleus. Moreover, exosome binding under the employed purification scheme was more robust for hRRP6. Therefore, in order to investigate the protein-protein interaction network of the human nuclear exosome, we first used hRRP6 as the bait in co-IP experiments. To this end, a Flp-In T-Rex HEK293 cell line stably expressing a tetracycline (tet) inducible and C-terminally FLAG-tagged version of hRRP6 was constructed. Specific hRRP6 interaction partners were determined using stable isotope labeling in cell culture (SILAC) methodology (Ong et al., 2003), followed by hRRP6-FLAG co-IP and high-resolution MS analysis. Induction conditions leading to only modest hRRP6 overexpression and the presence of the bait protein in the FLAG IP eluate were verified by western blotting analysis (Fig. S1A). To minimize RNA-dependent interactions, hRRP6-, and all other subsequent, purifications were conducted in the presence of RNase A.

The SILAC/MS approach classifies interactors by specificity (the SILAC ratio between peptide intensities of the bait-induced vs. un-induced samples) and protein abundance estimated from the sum of peptide signal intensities of a given protein normalized to its molecular mass (Fig. 1A). As expected, hRRP6 co-purified all nine core subunits of the exosome as well as C1D, hMPP6 and hMTR4 (Fig. 1A, 1B; Table S1). Also, in agreement with previous results, a less abundant - but highly specific - association of hDIS3 was detected. Interestingly, besides hMTR4, two other putative homologs of yeast TRAMP components, hTRF4-2 and ZCCHC7, were

identified, along with nucleolar WD40-proteins, with high SILAC ratios (Fig. 1A; Table S1) (Gallenberger et al., 2010; McMahon et al., 2010). This implies the existence of a human counterpart of yeast TRAMP (see below).

hMTR4 has previously been reported to interact with the exosome only by indirect studies (Schilders et al., 2007; Tomecki et al., 2010). Our MS data demonstrated hMTR4 co-purification with hRRP6-FLAG to near stoichiometric levels (Fig. 1A; Table S1), a salt-sensitive affinity, which was also evident from commassie-stained protein gels of the hRRP6-FLAG eluate (Fig. 1B). To investigate whether hRRP6 help facilitate hMTR4 interaction with the nuclear exosome, we conducted core component (hRRP41-FLAG) co-IP analysis from HEK293 cells in which hRRP6 had been depleted by RNAi (Fig. S1B), and compared it to a co-IP from control siRNA-treated cells. Upon hRRP6 siRNA administration, levels of the protein in the eluate, as determined by MS, dropped to ≈30% of that of exosome core components (Fig. 1C). This drop was paralleled by a decrease in hMTR4 (Fig. 1C). In addition, levels of other exosome co-factors decreased (MPP6), or completely disappeared (C1D), concomitantly. Thus, hRRP6 appears to stabilize the association of hMTR4, as well as C1D and MPP6, with the exosome core (see Discussion). We note, however, that under physiological conditions, hMTR4 is likely able to interact/activate the exosome core hRRP6-independently. This is because hMTR4, but not hRRP6, is central for proper 5.8S rRNA 3'end processing ((Schilders et al., 2007); and see below).

Identification of the hMTR4-containing NEXT complex

Given its strong interaction with the nuclear exosome and its predicted central position as an exosome activator, we next characterized hMTR4 interaction partners by the SILAC/MS approach. To this end, physiological levels of hMTR4-FLAG was

stably expressed, and the presence of the bait protein in the FLAG IP was evaluated (Fig. S1C). In a SILAC experimental approach, the hMTR4-FLAG bait efficiently co-purified the entire nuclear exosome core as well as hRRP6, C1D and MPP6 (Fig. 2A; Table S2). Interestingly, the hMTR4-FLAG co-IP disclosed a set of new and highly specific interaction partners harboring putative RNA recognition motifs, while hTRF4-2 and ZCCHC7 only became detectable upon increasing the scale of the experiment in a label-free setting (Fig. S1D; Table S3, see Materials and Methods). Some of these new interaction partners were previously localized to the nucleus: ZCCHC8, RBM7, ARS2 and CBP80 (Gruber et al., 2009; Gustafson et al., 2005; Nielsen et al., 2009; Wilson et al., 2008), whereas others are uncharacterized proteins, seemingly differentially localized between the non-nucleolar: ZC3H18 and C14orf102, and the nucleolar: ZFC3H1 and ZCCHC7, part of the nucleus (www.uniprot.org, www.lamondlab.com).

To uncover the more stably associated factors, we first measured protein IP levels after extracts from induced and un-induced samples were mixed (mixed extract 'ME') prior to the IP reaction, and compared it to IP levels obtained using the normal procedure of mixing FLAG-affinity beads (mixed beads 'MB') before co-elution (Fig. 2B). Since extract mixing allows for the exchange of labeled and non-labeled proteins, this experimental strategy assays the stability of interactions. Indeed, while hMTR4 association with nuclear exosome components was efficiently exchanged by the ME procedure, the RBM7, ZFC3H1 and ZCCHC8 proteins all purified with similar efficiencies whether the ME or the MB approach was applied (Fig. 2C). As hMTR4 co-purified ZCCHC8 with very high specificity and protein abundance (Fig. 2A), we also assayed complex formation by a reverse co-IP experiment, employing HEK293 cells stably expressing ZCCHC8-FLAG at physiological levels as the bait (Fig. S1E).

Gratifyingly, in addition to the entire nuclear exosome, MPP6 and C1D, ZCCHC8 also co-purified hMTR4 and RBM7; both with a very high efficiency and specificity (Fig. 2D and S1F; Tables S4 and S5). Moreover, analysis revealed that while exosome components could be 'chased' by mixing extracts, the association of ZCCHC8 with hMTR4 and RBM7 remained unaffected (Fig. 2E). Consistently, conducting hMTR4-FLAG or ZCCHC8-FLAG purifications at stringent conditions of 500mM NaCl resulted in the specific enrichment of hMTR4/ZCCHC8/RBM7 trimeric complexes (Fig. S2A and S2B; Table S6 and S7). Finally, we performed purification of a stably integrated RBM7-EGFP fusion construct, which revealed a near stoichiometric interaction with hMTR4 and ZCCHC8 (Fig. 2F). Collectively, these analyses demonstrate that hMTR4, ZCCHC8 and RBM7 form a stable trimeric complex, which we have named the Nuclear EXosome Targeting (NEXT) complex.

Sub-nuclear partitioning of exosome co-factors

To complement the proteomic analyses, we next examined the subcellular localization of NEXT components, and also included hTRF4-2 and ZCCHC7 in this analysis. Both N- and C-terminal EGFP fusions were generated and visualized by confocal microscopy in transiently transfected HeLa- and in stably transfected HEK293-cells, respectively. Generally, the positioning of the EGFP-tag did not affect localization of factors. Noticeably, ZCCHC8 and RBM7 both localized strictly to the non-nucleolar part of HeLa and HEK293 nuclei (Fig. 3A, 3B and S3A). Moreover, a revisit of the distribution of hMTR4 confirmed its previously reported nuclear localization with nucleolar accumulation, resembling the distributions of hRRP6, MPP6 and C1D (Schilders et al., 2007; Tomecki et al., 2010). Taken together with the co-IP analyses, we therefore suggest that the non-nucleolar pool of hMTR4

associates with ZCCHC8 and RBM7 to form the NEXT complex, whereas nucleolar hMTR4 is, among other factors, complexed with hRRP6, MPP6 and C1D.

Turning to putative TRAMP homologs, a remarkably strict nucleolar localization of ZCCHC7 was observed (Fig. 3A, 3B, and S3A). This result was confirmed using anti-ZCCHC7 antibodies for immuno-localization analysis of HeLa cells, a signal which disappeared upon depletion of the ZCCHC7 protein by RNAi (Fig. S3B). The nucleolar localization of ZCCHC7 is consistent with its association with factors previously reported to be nucleolar (see below). Finally, examination of hTRF4-2-EGFP expressing cells demonstrated its nuclear localization with nucleolar accumulation, fairly similar to hMTR4 (Fig. 3A, 3B, and S3A). This finding is consistent with localization data obtained for the closest Trf4/5p homolog in fission yeast, Cid14, and for DmTrf4 in *D. melanogaster* (Nakamura et al., 2008; Win et al., 2006). It is also compatible with the recent finding that hTRF4-2 is involved in the adenylation of rRNA degradation products (Shcherbik et al., 2010), but contrasts the unexpected cytoplasmic localization previously reported (Mullen and Marzluff, 2008).

To further characterize these putative nuclear exosome co-factors, we determined their sedimentation profiles in a 5%-40% glycerol gradient, separating whole cell extracts of HEK293 cells. Individual fractions of the gradient were subsequently analyzed by western blotting using available antibodies. The human exosome core has previously been reported to sediment into two differently sized pools (Mitchell et al., 1997; van Dijk et al., 2007), which we also found by probing fractions with hRRP40 and hRRP45 antibodies (Fig. 3C). Interestingly, hDIS3 was virtually excluded from the high molecular weight portion of the gradient, where instead hRRP6 accumulated. In contrast, hDIS3 was found in the light fractions, where hRRP6 was relatively less present. This rough separation of nuclear exosome sub-

populations parallels well the nucleolar exclusion and accumulation of hDIS3 and hRRP6, respectively (Tomecki et al., 2010). A similar partitioning of ZCCHC8 and ZCCHC7 was observed, with the former primarily present in the hDIS3 containing fractions, and the latter accumulating in the hRRP6 containing fractions (Fig. 3C). Again, this correlates well with the sub-nuclear localization of these factors. We were unable to probe the gradient fractions for RBM7 and hTRF4-2 as antibodies towards these factors were not available.

Interaction profiles of human putative TRAMP homologs

hMTR4, hTRF4-1, hTRF4-2 and ZCCHC7 display a domain composition similar to their putative yeast counterparts (Fig. 4A; for full alignments see Fig. S4A-C). Given their specific presence in the hRRP6-FLAG- and hMTR4-FLAG-precipitates (Fig. 1A and S1D), we focused on ZCCHC7 and hTRF4-2 for further label-free interaction studies. As in earlier purifications, moderate induction levels were used (Fig. S4D, lower left, ZCCHC7 was tested – for hTRF4-2 no antibodies were available) and the presence of bait proteins in the FLAG IPs was verified. The strongest indication of a human TRAMP complex comes from the ZCCHC7-FLAG bait purification, where hMTR4 and hTRF4-2 were specifically present in high amounts together with exosome components (Fig. 4B; Table S8). Moreover, in agreement with its localization, the ZCCHC7-FLAG IP revealed WDR36, WDR3, PWP2 and TBL3 proteins that are involved in rRNA biogenesis (Gallenberger et al., 2010). These proteins were also present in the hTRF4-2-FLAG eluate, as was hRRP6, hMTR4 and ZCCHC7 (Fig. 4C and 4D; Table S9). In addition, hTRF4-2 also interacted with a subset of splicing factors. This dual interaction profile with assigned nucleolar and non-nucleolar proteins likely reflects the sub-nuclear localization of hTRF4-2 (Fig. 3).

Although the ZCCHC7 and hTRF4-2 interaction analysis indicated the presence of a human TRAMP complex, we were not able to obtain enough material to verify its existence by SDS-PAGE and protein staining. Instead, we conducted western blotting analysis and confirmed the co-IP/MS data that ZCCHC7 and hTRF4-2 interact with each other and with hRRP6 in a salt-sensitive manner (Fig. 4D).

Substrate preferences of human exosome co-factors reflect their sub-nuclear localizations (NEXT components)

Provided that the proteins characterized in this paper are true co-factors of the human exosome, their removal should affect levels of its nuclear substrates. Hence, to examine the *in vivo* activity of NEXT components, hTRF4-2 and ZCCHC7, we depleted these proteins in HeLa cells using RNAi (Fig. 5A). In the case of RBM7 and hTRF4-2 where antibodies were not available, we tested the siRNA-directed depletion efficiency on cell lines stably expressing RBM7-EGFP (Fig. 5A, bottom left) or hTRF4-2-FLAG (Fig. 5A, bottom right). All siRNAs exhibited robust knock down efficiencies. In addition, and as previously reported for the hRrp40 knock down, which co-depletes hRrp6 (Kammler et al., 2008; Tomecki et al., 2010), depletion of key proteins in some cases decreased levels of others; i.e. hMTR4 knock down co-depleted ZCCHC8 and hRRP6 (Fig. 5A, lane 4) and administration of siRNA against hTRF4-2 caused decreased levels of ZCCHC7 (Fig. 5A, lane 3). This possibly reflects the tight individual interactions of these factors.

As the NEXT complex is confined to the non-nucleolar part of the nucleus, we turned to PROMPTs (Preker et al., 2008). These transcripts are degraded by either of the two nuclear nucleolytic exosome subunits hRRP6 or hDIS3, the latter of which is excluded from nucleoli (Tomecki et al., 2010). We therefore surmised that

exosome-directed PROMPT-removal cannot be nucleolar. In agreement with previous studies (Preker et al., 2008; Tomecki et al., 2010), selected PROMPTs were markedly stabilized in hRRP40 singly- as well as hDIS3/hRRP6 double-depleted cells, whereas individual depletion of hDIS3 or hRRP6 had smaller effects (Fig. 5B). Interestingly, depletion of NEXT complex components also resulted in robust PROMPT stabilization, whereas hTRF4-2- and ZCCHC7-depletions had no effect. Increased PROMPT levels were most pronounced in hMTR4-depleted samples, probably reflecting the pleiotropic effects of this knock down. We conclude that the NEXT complex cooperates with the nuclear exosome to remove PROMPTs from the non-nucleolar parts of human cell nuclei.

Substrate preferences of human exosome co-factors reflect their sub-nuclear localizations (ZCCHC7 and hTRF4-2)

Due to the nucleolar localizations of ZCCHC7 and hTRF4-2, we next turned to substrates assumed to be degraded in this sub-compartment. hTRF4-2 is involved in the adenylation of nascent 47S rRNA degradation intermediates (Fig. 6A), appearing as a result of treatment with a low concentration of Actinomycin D (Shcherbik et al., 2010). Presumably the drug triggers rRNA degradation by inhibiting RNA polymerase I activity, and since this is the hallmark of nucleolar assembly, we inferred that hTRF4-2 action may occur herein. To visualize adenylation of these pre-rRNA degradation intermediates, we adopted the assay of Shcherbik et al. and subjected total RNA from Actinomycin D treated cells to dT-primed semi-quantitative PCR followed by Southern blotting analysis using a radio-labeled 5'ETS specific probe (Fig. 6B). In accordance with published data, depletion of hRRP40 or hRRP6 resulted in increased levels of PCR products corresponding to adenylated 5'ETS

fragments, as did hMTR4-depletion (Fig. 6C). hDIS3 knockdown had no effect, implying that 5'ETS adenylation is indeed occurring in the nucleolus. Importantly, depletion of both hTRF4-2 and ZCCHC7 resulted in decreased levels of 5'ETS product as compared to the EGFP control (Fig. 6C, compare lane 1 with lanes 6 and 9), whereas ZCCHC8 and RBM7 depletions had no effect. Even more pronounced, co-depletion of hTRF4-2 or ZCCHC7 in the hRRP40- or hMTR4-depleted backgrounds, yielded a substantial down-regulation of the otherwise increased 5'ETS signals (Fig. 6C, compare lane 2 with lanes 7 and 10, or lane 5 with lanes 8 and 11). We conclude that ZCCHC7 and hTRF4-2 are co-factors of the human nucleolar exosome and that although ZCCHC7 has no adenylation activity of its own, it possibly aids hTRF4-2 in this function. Moreover, hMTR4 appears dispensable for adenylation of 5'ETS fragments, suggesting that a putative hTRF4-2/ZCCHC7 dimer may suffice to bind and adenylate target RNA, whereas hMTR4 facilitates recruitment of the exosome for transcript degradation.

Finally, we tested the effects of factor depletions on nuclear processing of the thoroughly studied exosome substrate 5.8S rRNA. As previously observed (Tomecki et al., 2010), hRRP40 and hRRP6/hDIS3 depletions caused the appearance of slower migrating 5.8S rRNA species when assayed by northern blotting analysis using a probe specific for the 3'extended region (Fig. 6D). Interestingly, hMTR4 depletion also yielded a robust 3'end processing defect, while neither ZCCHC8, RBM7, hTRF4-2 nor ZCCHC7 knock down showed a noticeable phenotype. It therefore seems that 5.8S rRNA processing requires the nuclear exosome complexed with hMTR4, whereas the NEXT complex and the putative TRAMP homologous factors are dispensable. Moreover, the partial phenotype seen upon

hDIS3 depletion argues that 5.8S rRNA 3'end processing in human cells occurs - at least in part - outside nucleoli.

Discussion

A vast amount of work on the *S. cerevisiae* exosome has convincingly demonstrated the need for co-factors to efficiently deal with its many cellular RNA substrates. Here, we uncover an interaction network of the human nuclear exosome, revealing a set of new partners, harboring an unanticipated complexity of composition and compartmentalization. Our data position hMTR4 as a central component in the coupling between the ribonucleolytic activity of the exosome and its other co-factors (summarized in Fig. 7). In sum, we propose that hRRP6 helps stabilize the tethering of hMTR4 to the exosome core, and that hMTR4 provides the link to compartment-specific activators/adaptors. Thus, similar to the ribonucleolytic activities of the human exosome, its nuclear co-factor complexes are also differentially distributed (Staals et al., 2010; Tomecki et al., 2010).

In *S. cerevisiae*, Mtr4p is indispensable for all known nuclear exosome activities, including 5.8S rRNA processing, which does not require other TRAMP complex components (Allmang et al., 1999; Bird et al., 2005; LaCava et al., 2005; Torchet et al., 2002; van Hoof et al., 2000). Our data suggest a parallel situation in human cells; i.e. depletion of hMTR4 causes, in contrast to other examined exosomal co-factors, an accumulation of 5.8S rRNA precursor species akin to that resulting from depletion of the hRRP40 core exosome subunit (Fig. 6C). Moreover, hMTR4 also exerts 'exosome core-like activity' on the analyzed PROMPT and 5'ETS substrates (Fig. 5B and 6B). Taken together with our data, that hRRP6 co-purifies hMTR4 with the exosome core at near stoichiometric levels (Fig. 1A), it seems appropriate to consider hMTR4 an integral activator of the human nuclear exosome. In further support of this notion, the sub-nuclear distributions of hMTR4, hRRP6, and the core

component hRRP45 (PM/Scl-75) are strikingly similar (Schilders et al., 2007). We note that Mtr4p also co-purifies with Rrp6p in yeast, thus, making a similar scenario possible in this organism (Peng et al., 2003). It is unlikely, however, that *in vivo* hRRP6 is the only factor involved in the tethering of hMTR4 to the exosome core as in both yeast and human cells, hRRP6 depletion yields relatively mild phenotypes on some substrates, e.g. 5.8S rRNA, as compared to hMTR4- or exosome core component-depletion (Fig. 6D, (Allmang et al., 1999; de la Cruz et al., 1998; LaCava et al., 2005; Schilders et al., 2007)). Thus, hMTR4 may also be involved in preparing substrates for the exosome, independent of its direct association.

The NEXT complex

S. cerevisiae Mtr4p is in excess of other exosome components and co-factors (Ghaemmaghami et al., 2003). Our co-IP experiments suggest a similar situation in human cells; i.e. hMTR4 is purified by hRRP6-FLAG in stoichiometric amounts with exosome components (Fig. 1A), but is in excess over same factors when hMTR4-FLAG is used as the bait (Fig. 2A). This may indeed enable hMTR4 to 'explore' the nucleus for additional co-factors, some of which are likely to serve as adaptors between the exosome and its substrates. Here, we describe the identification of the NEXT complex, consisting of hMTR4, ZCCHC8 and RBM7. This trimeric complex can be purified to near homogeneity at high salt conditions when RBM7-EGFP is used as the bait (Fig. 2F), and is very stable when challenged with exogenous extract in the ME/MB experimental scheme (Fig. 2C and 2E). NEXT factors also co-purify to near stoichiometry when physiological levels of ZCCHC8-FLAG are used as bait (Fig. 2D). However, consistent with the idea that hMTR4 is also engaged with other exosome co-factors, with the exosome itself and perhaps even with exosome-

unrelated proteins, RBM7 and ZCCHC8 are detected only as sub-stoichiometric partners when physiological levels of hMTR4-FLAG are used as bait (Fig. 2A).

We suggest that NEXT constitutes a non-nucleolar hMTR4-containing complex (Fig. 7), which targets, among other possible substrates, PROMPTs for rapid exosomal turnover. This is because nuclear ZCCHC8 and RBM7 are excluded from nucleoli (Fig. 3), and because their depletions result in PROMPT stabilization levels, that are reminiscent of those obtained when depleting hRRP40 or hRRP6/hDIS3 (Fig. 5B). Since RBM7 and ZCCHC8 harbor an RRM and a Zn-knuckle domain, respectively, it is possible that they provide substrate-targeting activity. Their tight assembly with hMTR4 in the NEXT complex could then facilitate the efficient funnelling of e.g. PROMPTs into the exosome. Such a model suggests the existence of a divergent pathway for nuclear ncRNA turnover in higher eukaryotes. As PROMPTs share many characteristics with *S. cerevisiae* CUTs, the participation of putative TRAMP homologs in PROMPT decay might have been expected. However, ZCCHC7 depletion has no discernable effect on PROMPT levels (Fig. 5B). Moreover, although hTRF4-2 can adenylate PROMPT 3'ends (Preker et al., submitted), this activity is not required for RNA degradation per se (Fig. 5B). Rather, PROMPT 3’ends, accumulating in the absence of a functional exosome, can provide substrates for hTRF4-2, consistent with its presence also in the non-nucleolar part of the nucleus. This is in contrast to *S. cerevisiae*, where both Trf4p and Air2p are directly required for the decay of CUTs (Wyers et al., 2005). Another difference between systems is the apparent lack of a human Nrd1p/Nab3p/Sen1p complex, which couples the transcription termination of CUTs to their rapid turnover (Lykke-Andersen and Jensen, 2006). Based on sequences, there are no strong candidate homologs of Nrd1p and Nab3p in the human genome. It thus remains an open question how

tightly the NEXT-directed decay of PROMPTs is coupled to the act of PROMPT transcription. As most human snoRNAs are cleaved out of larger precursor RNAs, in contrast to *S. cerevisiae* snoRNAs that are often transcribed from independent loci, it may be that the requirement of a Nrd1p/Nab3p/Sen1p-like complex to couple ncRNA transcription directly to exosomal processing/decay has been lost during evolution.

Interestingly, ZCCHC8 was previously found to be a target of the glycogen synthase kinase 3 (GSK-3) and to co-purify RBM7 and hMTR4, although no link to the RNA exosome was made (Gustafson et al., 2005). Moreover, RBM7 reportedly interacts with splicing factors (Guo et al., 2003). The relevance of these observations for the role of NEXT in RNA biology and exosomal targeting remains to be addressed.

A TRAMP complex in human cells?

Much effort has gone into the identification of TRAMP subunit homologs in higher eukaryotes, but apart from predictions, only little experimental support has been provided (Houseley and Tollervey, 2008). Here, we identify for the first time putative human TRAMP subunits hTRF4-2 (PAPD5) and ZCCHC7 (hAIR2) using hRRP6 (Fig. 1A) or hMTR4 (Fig. S1D) as purification baits. Validation by western blotting analysis verifies that these proteins indeed interact with the nuclear exosome and hMTR4, albeit less strongly than NEXT components (Fig. 4D). Consistently, hTRF4-2 is reportedly involved in the adenylation of rRNA degradation products (Shcherbik et al., 2010), an observation recapitulated in this paper and extended to also be valid for ZCCHC7 (Fig. 6C). As opposed to its assembly into the NEXT complex, we do not have firm proof that hMTR4 interacts directly with neither ZCCHC7 nor hTRF4-2. However, in favor of such a scenario, hMTR4 protein abundance was high in both

ZCCHC7-FLAG- and hTRF4-2-FLAG-IPs (Fig. 4B and 4C). Hence, we predict the existence of a nucleolar human 'TRAMP-like' complex (Fig. 7), which may even contain additional components like WDR3, WDR36, PWP2 and TBL3, scoring with similarly significant protein efficiencies in ZCCHC7-, hTRF4-2- and hMTR4-FLAG-precipitations (Fig. 4B, 4C and Fig. S1D). The exact composition of such complex(es) awaits further characterization.

Our reported nuclear localization of hTRF4-2 contrasts that reported by Mullen et al. (Mullen and Marzluff, 2008), who found the protein to be mainly cytoplasmic, a finding challenged by recent functional studies (Schmidt et al., 2010; Shcherbik et al., 2010). The hTRF4-2 clone used in this study exhibits a higher degree of conservation when compared to other vertebrate genomes (see Materials and Methods), and fusing it to EGFP, yielded the presented localization. Moreover, the amino acid composition of this isoform is consistent with the hTRF4-2 peptides obtained from both the ZCCHC7- and hMTR4-co-IPs, and we note that our hTRF4-2 IP also yields factors that are consistent with a nuclear function. Taken together, this strongly suggests that the present clone expresses physiologically relevant hTRF4-2. The functional relevance of hTRF4-2 outside nucleoli remains to be investigated, but the consistent presence of splicing factors in the hTRF4-2 co-IP may link the protein to pre-mRNA biology.

Additional targeting complexes of the nuclear human exosome?

Our data imply that additional nuclear exosome co-factors may exist. Most prominently present in the hMTR4- and ZCCHC8-FLAG-IPs are the Zn-knuckle proteins ZFC3H1, ZC3H18 and ARS2 (Fig. 2A, Fig. 2D, Fig. S1D, Fig. S1F and Fig. S2A). Interestingly, ZFC3H1 scores high for both specificity and abundance in the

hMTR4 IP even when conducted in 500mM NaCl (Fig. S2A). ZC3H18 is significantly present in the ZCCHC8 IP (Fig. 2D), indicating a non-nucleolar localization. Future work will focus on delineating the nature of possible RNA substrates for these proteins. Finally, both hMTR4- and ZCCHC8-FLAG baits consistently co-purify the ARS2 protein together with one or both of the cap-binding proteins CBP20 and CBP80 (Fig. 2A, Fig. 2D, Fig. S1D and Fig.S1F). Murine and *Drosophila* ARS2 was recently suggested to link CBP20/CBP80 to the RNAi system, possibly through the biogenesis of miRNA (Gruber et al., 2009; Nielsen et al., 2009; Sabin et al., 2009; Wilson et al., 2008). Our finding may therefore link the human exosome with miRNA metabolism.

The complexity and range of reported RNA exosome substrates have steadily increased since the first discovery of the *S. cerevisiae* complex (Mitchell et al., 1997). Most, if not all, nuclear RNA 3'ends have, at some physiological condition, a chance of encountering the exosome, posing the question how these substrates are targeted for processing or decay. Although the rules of such targeting as well as the mechanisms underlying exosome activation are not yet well understood, this work revealing a set of new co-factors should pave the way for such analysis in human cells.

Materials and Methods

Plasmids and cloning

Plasmids used in the study are listed in Table S10. Coding sequences were amplified by PCR from a HEK293 cDNA library using oligonucleotides listed in Table S11, and cloned into the BamHI/XhoI sites of pcDNA5/FRT/TO-FLAG (Invitrogen) using standard procedures . Tetracycline inducible cell lines stably expressing FLAG or EGFP fusions were generated according to the manufacturer using the Flp-In™ T-REx™ system (Invitrogen). Optimal expression conditions were tested for each construct using different concentrations (10-1000ng/ml) of tetracycline.

To amplify cDNA encoding hTRF4-2 HeLa- and HEK293-RNA was used. The longest cDNA variant was sub-cloned to obtain FLAG- and EGFP- protein fusions (as described above). In comparison to the previously localized isoform of hTRF4-2 (Q8NDF8) (Mullen and Marzluff G&D 2008), the one used here (submitted to UniProt) includes two insertions: (i) 12 amino acids in close proximity to the signal peptide (N-terminus) and (ii) 47 amino acids in the C-terminal region of the protein.

SILAC and label-free co-IPs

In SILAC experiments proteins were labelled with stable isotopes in cell culture. HEK293 Flp-In T-Rex cell lines harbouring FLAG-tagged versions of hRRP6, ZCCHC8 or hMTR4 were cultured for a minimum of five doublings in custom-made DMEM SILAC media, containing 15% dialyzed FBS (Gibco), 2mM L-glutamine, 100U/ml penicillin and 100ug/ml streptomycin. Subsequently, cells were grown for 24h in media containing Lys0 ($^{12}C_6{}^{14}N_2$) and Arg0 ($^{12}C_6{}^{14}N_4$), or Lys4: ($^{2}H_4$) and Arg6 ($^{13}C_6{}^{14}N_4$) (Sigma-Isotec), fresh media was added and the pool of cells growing on

labelled amino acids was induced with tetracycline (hRRP6 – 30ng/ml, hMTR4 – 30ng/ml, ZCCHC8 – 10ng/ml). 24h later, cells from one 145mm plate were collected and washed in 0,75ml of PBS (Gibco) and collected in RSB100 buffer (10mM Tris/HCl pH 7.4, 100mM NaCl, 2.5mM MgCl2), containing 0.5% Triton X100 and protease inhibitors (Roche). Cells were gently lysed by sonication: 3x10sek, 20W (Branson 250) and centrifuged (4000g, 15min) at 4°C. Supernatants were treated with RNase A (100ug/ml) for 15min on ice and centrifuged (16000g, 5min) at 4°C. 'Mixed extracts (ME)' and 'mixed beads (MB)' experiments were set-up as described in the results section and loaded onto agarose anti-FLAG (M2) beads (Sigma). After 3h of incubation, beads were washed 4 times with RSB100/0.5% Triton X100. For the MB approach, beads were pooled in one tube, and both MB and ME were washed 4 times with RSB100. For high-salt purifications all washing steps were performed in RSB500 (500mM NaCl). Proteins were eluted with FLAG peptide (0.5 mg/ml) in TBS (Sambrook and Russell, 2001). Additional elution was done by incubation with 2 x SDS loading buffer. Before MS analyses samples were analysed SDS-PAGE followed by silver staining (data not shown) and western blotting. 1/100 of the initial input and 1/10 of FLAG eluate, respectively, were loaded on gels.

Sample preparation, MS analyses and data treatment

Prior to MS analysis eluates were denatured with 8M Urea and digested in solution by endoproteinases: LysC in 6M Urea, 50 mM ammonium bicarbonate buffer, pH 7.8 (0.1AU/mL, Wako) for 3h at room temperature and trypsin (Promega) over night at 37°C. Released peptides were reduced in 10mM dithiotreitol (DTT) for 30min at RT and alkalized in 55mM iodoacetamide for 20min at room temperature. Finally, peptides extracted with 1% trifluoroacetic acid (TFA) and concentrated on home-

made reverse-phase C18 columns (prewashed with methanol) were eluted with 80% acetonitrile/0.5% TFA, then dried and analyzed by LC-MS.

MS and data analyses were performed as previously described (Tomecki, et al. 2010). The LTQ-Orbitrap mass spectrometer was operated in a mode, which provides high-resolution of ion spectra (m/z 300–1500, resolution 60000 and ion accumulation to a target value of $5x10^6$ ions). MaxQuant software (version 1.0.13.13) was used to extract peptide ion and fragment ion m/z intensity signals from the mass spectra (Cox and Mann, 2008), which were submitted to the Mascot program (Matrix Science) for database searches (Human IPI sequence database). The same software was used for calculation of peptide isotope ratios as well as evaluation of the certainty of peptide identification using false discovery rate analysis.

Label free quantitation was done using the MaxQuant software. Peptide m/z signal intensity was found summing intensities over the entire elution of the peptide, and protein intensity as the sum of intensities for all peptides representing the protein. Proteins included in Tables S1-9 provide hits identified by a false discovery rate of 0.01 derived by decoy database searching, and only unique peptides were used for the quantitation. The previously reported non-specific binders also detected in a ‘bead proteome’ were removed from the datasets (Tomecki et al., 2010).

Purification of the NEXT complex

HEK293 RBM7-EGFP cells were induced by 10ng/ml of tetracycline. The standard co-IP protocol was scaled up to include ten 145mM plates and the entire procedure was performed in high salt conditions (RSB500). Elution was performed with 0.1M glycine pH 2.5, followed by neutralization with 1M Tris/HCl pH 8.0. 1/10 of the eluate was loaded on the gel.

Protein alignments and motif finding

Protein sequences (Table S12) were loaded into the CLC Main workbench 5.6.1 software (www.clcbio.com). Alignments were created using the create alignment tool with a gap open cost of 10 and a gap extension cost of 1. Protein motifs were found using the pfam domain search, using the 100 most common motifs and a significance cut-off at E=1.

Localization studies

Localization analyses were performed essentially as described (Tomecki et al., 2010). For localization of EGFP-tagged proteins in HeLa cells, the cells were seeded on 6-well Lab-Tek® Chamber Slides (Nunc), and 12h later transfected with appropriate constructs using a standard transfection protocol. Test media was supplemented with tetracycline to induce protein expression. 24h later localization experiments were performed directly on living cells, or indirectly by immunofluorescence analysis of formaldehyde-fixed cells. Nuclei were stained with Hoechst 33342 and nucleoli were visualized by both phase contrast light and anti-fibrillarin antibodies (Abcam 1:150). Cells were visualized by confocal microscopy - *Olympus FluoView® FV10i* – using a 60x water-immersion objective (NA 1,2).

siRNA-mediated knock-downs and RT-qPCR

Transfections were carried out using 20 nM siRNA (Table 13) for 2 days and repeated for another 2 days both times using Lipofectamin2000 (Invitrogen). Five µg of total RNA was treated with 1U of DNase I (Invitrogen), reverse transcribed using 0.5µg of a dT primer, which was anchored at the 3'end and carried an adaptor at the

5’end (APVN) and Superscript II in a volume of 20µl. Dilutions were subjected to qPCR analyses on a Stratagene Mx3005P using Platinum SYBR Green (Invitrogen) and 0.3µM of oligonucleotides at an annealing temperature of 59°C. Controls lacking Superscript II showed a negligible background. A complete list of RT-qPCR primers is found in Table S14.

Western blotting analysis

Cells were treated with siRNA directed against the protein of interest and equal amounts of cell lysate, or whole cell extract, were subjected to 10% SDS PAGE, and subsequently analyzed according to standard procedures (Sambrook and Russell, 2001) using the following primary antibodies: monoclonal mouse anti-FLAG M2 (Sigma-Aldrich), polyclonal mouse anti-ZCCHC8 and polyclonal rabbit anti-hMTR4 (Abcam), polyclonal mouse anti-RRP40 and anti-EGFP (Santa Cruz biotechnology), polyclonal rabbit anti-RRP40 (courtesy of Dr. Ger Pruijn), polyclonal rabbit anti-DIS3 (Abnova), polyclonal anti-ACTIN and polyclonal rabbit anti-RRP6 (Sigma-Aldrich) and polyclonal rabbit anti-ZCCHC7 (Atlas antibodies). Anti-mouse and anti-rabbit IgGs coniugated with HRP (Dako) were used as secondary antibodies .

Glycerol gradient

Whole cell extracts were prepared by washing cells with PBS followed by scraping into RSB100 buffer, containing 0.5% Triton X-100 and protease inhibitor (one Complete, mini, EDTA-free, Protease Inhibitor cocktail (Roche) tablet per 10ml of buffer). Cell slurries were sonicated on ice using a Branson Sonifier 250 at setting 1 (output: ~20W) for 3x10 s, and subsequently centrifuged at 4000g for 15min at 4°C. The supernatant was loaded onto a 5%-40% (v/v) glycerol gradient, prepared in

gradient buffer (RSB100 containing 0.5% Triton X-100). The gradient was centrifuged essentially as described (van Dijk et al., 2007), only using a SW41 (Beckman) rotor, and collecting 21 fractions. These were precipitated by TCA, re-suspended in SDS load buffer, separated by SDS-PAGE and transferred to a nitrocellulose membrane for western blotting analysis.

rRNA analysis

Five µg of total RNA from cells treated with siRNA was run on a 7% denaturing polyacrylamide gel and analyzed by standard northern blotting procedures. ITS2 extensions and mature 5.8S rRNA were visualised using an *in vitro* transcribed RNA probe kindly provided by Dr. Ger Pruijn (Schilders et al., 2007) and a 5'radiolabeled 5.8S rRNA specific DNA oligo: 5'-GTGTCGATGATCAATGTGTCCTGCAATTCA, respectively.

To analyze 5'ETS degradation products, HeLa cells were treated with siRNAs as described above. Before harvest, the medium was replaced with RPMI containing 20 ng/ml Actinomycin D for 60min. RNA was harvested and cDNA was prepared as described above, but using an unanchored adaptor-carrying dT primer (AP). The 5'ETS region was amplified by 19 cycles of PCR, using a 5'ETS-specific forward primer and the Abridged Universal Amplification Primer (AUAP), containing the sequence of the adaptor. PCR products were run on a 1% agarose gel and analyzed by standard southern blot procedures using an internal probe against 5'ETS. PCR using primers designed to amplify a part of GAPDH mRNA was used as control. For primers used in these experiments see Table S11.

Acknowledgements

We thank Stepanka Vanacova, John LaCava, Joanna Kufel and Rafal Tomecki for critical comments on the manuscript and members of the A.D., J.S.A. and T.H.J. laboratories for stimulating discussions. Kasia Kowalska, Ger Pruijn and Christian K. Damgaard are acknowledged for sharing reagents and for experimental advice. This work was supported by the Danish National Research Foundation, the Danish Cancer Society and the Lundbeck- and Novo Nordisk Foundations (to T.H.J.); the Foundation for Polish Science Team Programme co-financed by the EU European Regional Development Fund, the Operational Program Innovative Economy 2007-2013, the project support Agreement POIG.02.02.00-14-024/08-00 and an EMBO installation grant (to A.D.), and the European Commission's 7th Framework Programme (grant agreement HEALTH-F4-2008-201648/PROSPECTS (to J.S.A.). M.L. was supported by a Boehringer-Ingelheim PhD fellowship. The authors declare that they have no competing financial interests.

Figure legends

Fig. 1. **hMTR4 interacts stoichiometrically with the exosome core**

(A) hRRP6-FLAG SILAC co-IP result plotted by relative protein abundance (total peptide intensity divided by molecular weight (MW)) out the x-axis and log SILAC ratio (intensity of peptides originating from the hRRP6- *vs.* control-IP) up the y-axis. Note disruption of the x-axis to accommodate all detected proteins in the plot. Different types of interaction partners are indicated by color coding and relevant protein names are displayed. The entire data set is specified in Table S1. The asterisk (at hRRP6) indicates the FLAG-tagged bait protein.

(B) SDS-PAGE analysis of IP eluates from tet-induced (hRRP6-FLAG expressing) and un-induced HEK293 cells. Protein band ID's were achieved by MALDI-TOF MS. The migrations of IgG heavy- and light-chains as well as the HSPA1A protein contaminant are indicated.

(C) MS determination of relative levels of the indicated proteins in hRRP41-FLAG IP eluates from HEK293 cells depleted for hRRP6 *vs.* non-depleted cells. The calculation is done by MaxQuant (Cox and Mann, 2008), and based on the intensity of peptides from label-free experiments.

Fig. 2. **Identification of the nuclear exosome targeting (NEXT) complex**

(A) hMTR4-FLAG SILAC co-IP result plotted and labeled as in Fig. 1A. High-specificity interactors with log SILAC ratio above 0.5 are indicated in orange. Note disruption of the x-axis to accommodate all detected proteins in the plot.

(B) Schematic outline of the two different SILAC purification strategies, 'mixed extracts' (ME) and 'mixed beads' (MB), to assay for dynamics of interactions. IP

experiments of differentially labeled samples are either carried out separately and mixing beads at the end (MB, left) or by mixing extracts and subjecting this material to common bead-binding and elution (ME, right). SILAC ratios that are constant between experimental strategies signify stable interactions.

(C) Interaction dynamics of most prominent hMTR4 binding partners. SILAC ratios are displayed for MB (black) and ME (red) experiments.

(D) ZCCHC8-FLAG co-IP result plotted and labeled as in Fig. 1A. The two groups of high-specificity (log SILAC ratio>0.5) and high-abundance (signal intensity/MW*10^6>100) interactors are indicated in orange and blue, respectively. Note disruption of the x-axis to accommodate all detected proteins in the plot.

(E) Interaction dynamics of most prominent ZCCHC8 binding partners displayed as in (C).

(F) The NEXT complex: RBM7-EGFP fusion protein was purified from HEK293 cells using stringent conditions (500mM NaCl) and eluate was analyzed by SDS-PAGE. The MS-identification of commassie stained bands is indicated. Asterisks indicate contaminants.

Fig. 3. **Differential nuclear partitioning of human exosome co-factors**

(A, B) Nuclear-localized hMTR4 and hTRF4-2 accumulate in nucleoli. ZCCHC7 strictly localizes to, and nuclear ZCCHC8 and RBM7 are excluded from, nucleoli. In (A), HeLa cells were transiently transfected with plasmids expressing the indicated proteins as C-terminal EGFP fusions. 12h post-transfection, protein expression was induced with tetracycline for 24h, cells were fixed and proteins were visualized by confocal microscopy. Fibrillarin staining served as a nucleolar marker and was overlayed with labeling of nuclei by Hoechst stain. In (B), HEK293 Flp-In T-REx cells

stably expressing N-terminally EGFP-tagged proteins were analyzed by live cell confocal microscopy. Protein expression was induced as above. Cells were visualized using phase contrast and overlaid with signal from EGFP fluorescence.

(C) ZCCHC8 and ZCCHC7 distribute in hDIS3- and hRRP6-containing low and high molecular weight glycerol gradient fractions, respectively. Western blotting analysis of 5%-40% glycerol gradient fractions of HEK293 cell extract, employing the indicated antibodies. Input material corresponding to 5% of the total cell extract was loaded in each of the two outer lanes of the gel.

Fig. 4. **Interaction profiles of human putative TRAMP homologs**

(A) Domain comparison of putative TRAMP subunits from *H. sapiens*, *D. melanogaster* and *S. pombe* with those of *S. cerevisiae* TRAMP components. Known domains are colored as indicated. For detailed sequence alignments see Fig. S4A-C.

(B, C) ZCCHC7- and hTRF4-2-FLAG co-IP results plotted and labeled as in Fig. 1A. Only here, label-free IP's of ZCCHC7 and hTRF4-2 were conducted and peptide signal intensities were calculated by the label-free algorithm in MaxQuant software using normalization to the control (uninduced cell line) IP. Likely due to post-translational modifications, ZCCHC7 peptides were underrepresented in both MS spectra. Note disruption of the x-axes to accommodate all detected proteins in the plots. Full label-free datasets are labeled in grey.

(D) Verification of interactions by western blotting analysis. The hRRP6-, hMTR4-, ZCCHC8-, ZCCHC7- and hTRF4-2-FLAG eluates obtained after purification in the presence of 100mM, or 500mM, NaCl were probed with anti-hMTR4-, -hRRP6-, -ZCCHC8-, -ZCCHC7- and -hRRP40-antibodies as indicated. Asterisk denotes band corresponding to hRRP6 from previous hybridization.

Fig. 5. **Substrate preference of NEXT reflects its sub-nuclear distribution**

(A) Western blotting analysis of whole cell extracts showing protein depletion upon the indicated siRNA administrations. Top panels: HeLa cells were treated with the indicated siRNAs and control cells were treated with EGFP siRNA. Membranes were probed using specific antibodies as indicated to the right. Anti-Actin antibody was used as a loading control. HEK293 cells expressing EGFP-tagged RBM7 (bottom left) or FLAG-tagged hTRF4-2 (bottom right) were treated with the indicated siRNAs. In the EGFP-RBM7 experiment, TEL/AML siRNA was used as control. Protein depletion was assayed using anti-EGFP or anti-FLAG antibodies as indcated.

(B) PROMPTs are stabilized in cells depleted for exosome- and NEXT complex-components. Total RNA harvested from HeLa cells subjected to the indicated siRNA transfections were analyzed by dT-primed RT-qPCR using amplicons for the indicated PROMPTs; ID numbers from left to right: 40-9, -14, -16, -18, -38, -31, -13, -52, -33, -2b (Preker et al. 2008; Table S14). Data are displayed as mean values normalized to control (EGFP siRNA-treated cells). All data are normalized to GAPDH RNA as an internal control. Error bars represent standard deviations from biological repeats (n=3). Note disruption of y-axis to accommodate all data in the plot.

Fig. 6. **Substrate preference of ZCCHC7 and hTRF4-2 reflects their sub-nuclear distributions**

(A) Schematic representation of the 47S rRNA transcript. Boxes indicate the mature rRNAs 18S, 5.8S and 28S, which are flanked by the external spacers (ETSs) and separated by the internal spacers (ITSs).

(B) Schematic outline of the 5'ETS RNA adenylation assay. Adenylated 5'ETS RNAs arising from Actinomycin D-induced 47S rRNA degradation are reverse transcribed with the indicated dT-adaptor oligo followed by limited PCR using the indicated '5'ETS-1' and 'adaptor' primers. PCR products are subjected to Southern analysis using the 5'ETS-2 hybridization probe.

(C) Adenylation of 5'ETS degradation fragments is compromised upon ZCCHC7 or hTRF4-2 depletion. Southern blotting analysis of RT-PCR products derived from total RNA harvested from cells subjected to the indicated knock downs and using the reagents indicated in (B). A representative experiment from three repeats is shown. As an internal control, RT-PCR using GAPDH specific primers was performed. Probe signals were quantified, normalized to GAPDH levels and plotted relative to EGFP controls.

(D) hMTR4 and the core exosome are important for 5.8S rRNA 3'end prcessing. Total RNA harvested from HeLa cells subjected to the indicated siRNA-mediated knock downs was subjected to northern blotting analysis using a radiolabeled ribo-probe targeting the ITS2 region (A). Mature 5.8S rRNA was visualized using a radiolabeled DNA oligo-probe. Probe signals arising from the 3'end extended species were quantified and plotted relative to EGFP controls.

Fig. 7. Sub-nuclear distribution of human nuclear exosome co-factors

Model overview of human nuclear exosome co-factors and their sub-nuclear localizations as derived from this study. The dually (nucleolar as well as non-nucleolar) localized hMTR4 (structure derived from its *S. cerevisiae* homolog (Weir et al., 2010) is centrally positioned and associates with the nuclear exosome (dashed arrows). In the non-nucleolar part of the nucleus, hMTR4 forms a stable trimeric

complex with ZCCHC8 and RBM7. This NEXT complex is excluded from the nucleoli, where hMTR4 instead cooperates with putative TRAMP homologous components ZCCHC7 and hTRF4-2. The latter is also present outside nucleoli.

Supplementary figure legends

Figure S1

(A) Western blotting analysis of hRRP6-FLAG SILAC mixed beads (MB) co-IP experiment. The analysis shows that the tagged protein was expressed at near endogenous level when induced with 30ng/ml of tetracycline. Input and eluate fractions were probed with α-RRP6 antibodies.

(B) Western blotting analysis of whole cell extracts showing hRRP6 depletion efficiency in tetracycline-induced cells, used for hRRP41 label-free co-IP. HEK293 cells were treated with siRNAs against hRRP6 and EGFP (control).

(C, E) Western blotting verification of hMTR4- and ZCCHC8-FLAG expression levels in cells induced with different concentration of tetracycline (top panel). The optimal expression conditions (closest to endogenous level, marked in red) were applied for subsequent experiments: SILAC mixed beads (MB) and mixed extracts (ME) co-IP (bottom panel; Fig. 2A, C), and label-free experiments (Fig. S1D, F ; S2A, B). Input and eluate fractions were probed with α-FLAG, and specific α-hMTR4 and α-ZCCHC8 antibodies, respectively.

(D, F) hMTR4- and ZCCHC8-FLAG label-free co-IPs performed in low stringent conditions (100mM NaCl). Results are plotted and labeled as in Fig. 2A. The entire dataset is specified in Table S3. Peptide signal intensities were calculated by the label-free algorithm in MaxQuant software, using normalization to the control (uninduced cell line) IP. Note disruption of the x-axes to accommodate all detected proteins in the plots. Names of high-specificity and high-abundance interactors were displayed. Full label-free datasets are labeled in grey.

Figure S2

(A, B) hMTR4 and ZCCHC8-FLAG label-free co-IPs performed in highly stringent (500mM) conditions. Results are plotted as in Fig. S1D with only NEXT components indicated. The calculations were performed as before (Fig. S1D, F).

Figure S3

(A) Intracellular localization of C-terminal EGFP-tagged components of the NEXT complex: ZCCHC8, RBM7 and hMTR; as well as hTRF4 and ZCCHC7. HEK293 cells stably expressing the fusion proteins were subjected to the standard immunofluoresce procedure followed by confocal microscopy. Hoechst stained nuclei and fibrillarin were overlayed as indicated.

(B) Nucleolar localization of ZCCHC7 protein in HeLa cells. The cells were subjected to α-ZCCHC7 immunostaining, which pattern was then overlaid with phase contrast light (left panel - nucleoli are pointed with arrows). Specificity of the ZCCHC7 signal was verified by treatment of HeLa cells with siRNA against ZCCHC7 or EGFP (control). Similar settings were used for visualizations.

Figure S4

(A-C) Multiple sequence alignments of yeast Air1p, Trf4p and Mtr4p with their closest homologs from human, fly and fission yeast, as determined by using Basic Local Alignment Search Tool (BLAST) on protein sequence. All alignments were done using the CLC main Main workbench 5.6.1 software, www.clcbio.com. For protein accession numbers used in this study see Table S2.

(D) Western blotting verification of ZCCHC7- and hTRF4-FLAG induction levels in label-free co-IPs. Cells were induced with the indicated concentration of tetracycline.

Conditions marked in red were chosen for MS analyses. Inputs and eluates were probed with α-FLAG and α-ZCCHC7 antibodies (there is no-available reagent to detect hTRF4-2).

References

Allmang, C., Kufel, J., Chanfreau, G., Mitchell, P., Petfalski, E., and Tollervey, D. (1999). Functions of the exosome in rRNA, snoRNA and snRNA synthesis. EMBO J *18*, 5399-5410.

Anderson, J.S., and Parker, R.P. (1998). The 3' to 5' degradation of yeast mRNAs is a general mechanism for mRNA turnover that requires the SKI2 DEVH box protein and 3' to 5' exonucleases of the exosome complex. EMBO J *17*, 1497-1506.

Bird, G., Fong, N., Gatlin, J.C., Farabaugh, S., and Bentley, D.L. (2005). Ribozyme cleavage reveals connections between mRNA release from the site of transcription and pre-mRNA processing. Mol Cell *20*, 747-758.

Brown, J.T., Bai, X., and Johnson, A.W. (2000). The yeast antiviral proteins Ski2p, Ski3p, and Ski8p exist as a complex in vivo. RNA *6*, 449-457.

Cox, J., and Mann, M. (2008). MaxQuant enables high peptide identification rates, individualized p.p.b.-range mass accuracies and proteome-wide protein quantification. Nat Biotechnol *26*, 1367-1372.

Cristodero, M., and Clayton, C.E. (2007). Trypanosome MTR4 is involved in rRNA processing. Nucleic Acids Res *35*, 7023-7030.

de la Cruz, J., Kressler, D., Tollervey, D., and Linder, P. (1998). Dob1p (Mtr4p) is a putative ATP-dependent RNA helicase required for the 3' end formation of 5.8S rRNA in Saccharomyces cerevisiae. EMBO J *17*, 1128-1140.

Dez, C., Dlakic, M., and Tollervey, D. (2007). Roles of the HEAT repeat proteins Utp10 and Utp20 in 40S ribosome maturation. RNA *13*, 1516-1527.

Etheridge, R.D., Clemens, D.M., Gershon, P.D., and Aphasizhev, R. (2009). Identification and characterization of nuclear non-canonical poly(A) polymerases from Trypanosoma brucei. Mol Biochem Parasitol *164*, 66-73.

Gallenberger, M., Meinel, D.M., Kroeber, M., Wegner, M., Milkereit, P., Bosl, M.R., and Tamm, E.R. (2010). Lack of WDR36 leads to preimplantation embryonic lethality in mice and delays the formation of small subunit ribosomal RNA in human cells in vitro. Hum Mol Genet *20*, 422-435.

Ghaemmaghami, S., Huh, W.K., Bower, K., Howson, R.W., Belle, A., Dephoure, N., O'Shea, E.K., and Weissman, J.S. (2003). Global analysis of protein expression in yeast. Nature *425*, 737-741.

Gruber, J.J., Zatechka, D.S., Sabin, L.R., Yong, J., Lum, J.J., Kong, M., Zong, W.X., Zhang, Z., Lau, C.K., Rawlings, J.*, et al.* (2009). Ars2 links the nuclear cap-binding complex to RNA interference and cell proliferation. Cell *138*, 328-339.

Guo, T.B., Boros, L.G., Chan, K.C., Hikim, A.P., Hudson, A.P., Swerdloff, R.S., Mitchell, A.P., and Salameh, W.A. (2003). Spermatogenetic expression of RNA-binding motif protein 7, a protein that interacts with splicing factors. J Androl *24*, 204-214.

Gustafson, M.P., Welcker, M., Hwang, H.C., and Clurman, B.E. (2005). Zcchc8 is a glycogen synthase kinase-3 substrate that interacts with RNA-binding proteins. Biochem Biophys Res Commun *338*, 1359-1367.

Houseley, J., and Tollervey, D. (2006). Yeast Trf5p is a nuclear poly(A) polymerase. EMBO Rep *7*, 205-211.

Houseley, J., and Tollervey, D. (2008). The nuclear RNA surveillance machinery: the link between ncRNAs and genome structure in budding yeast? Biochim Biophys Acta *1779*, 239-246.

Houseley, J., and Tollervey, D. (2009). The many pathways of RNA degradation. Cell *136*, 763-776.

Kammler, S., Lykke-Andersen, S., and Jensen, T.H. (2008). The RNA exosome component hRrp6 is a target for 5-fluorouracil in human cells. Mol Cancer Res *6*, 990-995.

LaCava, J., Houseley, J., Saveanu, C., Petfalski, E., Thompson, E., Jacquier, A., and Tollervey, D. (2005). RNA degradation by the exosome is promoted by a nuclear polyadenylation complex. Cell *121*, 713-724.

Lejeune, F., Li, X., and Maquat, L.E. (2003). Nonsense-mediated mRNA decay in mammalian cells involves decapping, deadenylating, and exonucleolytic activities. Mol Cell *12*, 675-687.

Lykke-Andersen, S., Brodersen, D.E., and Jensen, T.H. (2009). Origins and activities of the eukaryotic exosome. J Cell Sci *122*, 1487-1494.

Lykke-Andersen, S., and Jensen, T.H. (2006). CUT it out: silencing of noise in the transcriptome. Nat Struct Mol Biol *13*, 860-861.

Lykke-Andersen, S., Tomecki, R., Jensen, T.H., and Dziembowski, A. (2011). The eukaryotic RNA exosome: Same scaffold but variable catalytic subunits. RNA Biol *8*.

McMahon, M., Ayllon, V., Panov, K.I., and O'Connor, R. (2010). Ribosomal 18 S RNA processing by the IGF-I-responsive WDR3 protein is integrated with p53 function in cancer cell proliferation. J Biol Chem *285*, 18309-18318.

Milligan, L., Decourty, L., Saveanu, C., Rappsilber, J., Ceulemans, H., Jacquier, A., and Tollervey, D. (2008). A yeast exosome cofactor, Mpp6, functions in RNA surveillance and in the degradation of noncoding RNA transcripts. Mol Cell Biol *28*, 5446-5457.

Milligan, L., Torchet, C., Allmang, C., Shipman, T., and Tollervey, D. (2005). A nuclear surveillance pathway for mRNAs with defective polyadenylation. Mol Cell Biol *25*, 9996-10004.

Mitchell, P., Petfalski, E., Houalla, R., Podtelejnikov, A., Mann, M., and Tollervey, D. (2003). Rrp47p is an exosome-associated protein required for the 3' processing of stable RNAs. Mol Cell Biol *23*, 6982-6992.

Mitchell, P., Petfalski, E., Shevchenko, A., Mann, M., and Tollervey, D. (1997). The exosome: a conserved eukaryotic RNA processing complex containing multiple 3'-->5' exoribonucleases. Cell *91*, 457-466.

Mullen, T.E., and Marzluff, W.F. (2008). Degradation of histone mRNA requires oligouridylation followed by decapping and simultaneous degradation of the mRNA both 5' to 3' and 3' to 5'. Genes Dev *22*, 50-65.

Nakamura, R., Takeuchi, R., Takata, K., Shimanouchi, K., Abe, Y., Kanai, Y., Ruike, T., Ihara, A., and Sakaguchi, K. (2008). TRF4 is involved in polyadenylation of snRNAs in Drosophila melanogaster. Mol Cell Biol *28*, 6620-6631.

Nielsen, A.F., Gloggnitzer, J., and Martinez, J. (2009). Ars2 and the Cap-Binding Complex Team up for Silencing. Cell *138*, 224-226.

Ong, S.E., Foster, L.J., and Mann, M. (2003). Mass spectrometric-based approaches in quantitative proteomics. Methods *29*, 124-130.

Peng, W.T., Robinson, M.D., Mnaimneh, S., Krogan, N.J., Cagney, G., Morris, Q., Davierwala, A.P., Grigull, J., Yang, X., Zhang, W.*, et al.* (2003). A panoramic view of yeast noncoding RNA processing. Cell *113*, 919-933.

Preker, P., Nielsen, J., Kammler, S., Lykke-Andersen, S., Christensen, M.S., Mapendano, C.K., Schierup, M.H., and Jensen, T.H. (2008). RNA exosome depletion reveals transcription upstream of active human promoters. Science *322*, 1851-1854.

Reis, C.C., and Campbell, J.L. (2007). Contribution of Trf4/5 and the nuclear exosome to genome stability through regulation of histone mRNA levels in Saccharomyces cerevisiae. Genetics *175*, 993-1010.

Rougemaille, M., Gudipati, R.K., Olesen, J.R., Thomsen, R., Seraphin, B., Libri, D., and Jensen, T.H. (2007). Dissecting mechanisms of nuclear mRNA surveillance in THO/sub2 complex mutants. EMBO J *26*, 2317-2326.

Sabin, L.R., Zhou, R., Gruber, J.J., Lukinova, N., Bambina, S., Berman, A., Lau, C.K., Thompson, C.B., and Cherry, S. (2009). Ars2 regulates both miRNA- and siRNA- dependent silencing and suppresses RNA virus infection in Drosophila. Cell *138*, 340-351.

Sambrook, J., and Russell, D. (2001). Molecular cloning: a laboratory manual (2001) 3rd. Plainview (New York: Cold Spring Harbor Laboratories).

San Paolo, S., Vanacova, S., Schenk, L., Scherrer, T., Blank, D., Keller, W., and Gerber, A.P. (2009). Distinct roles of non-canonical poly(A) polymerases in RNA metabolism. PLoS Genet *5*, e1000555.

Schilders, G., and Pruijn, G.J. (2008). Biochemical studies of the mammalian exosome with intact cells. Methods Enzymol *448*, 211-226.

Schilders, G., van Dijk, E., and Pruijn, G.J. (2007). C1D and hMtr4p associate with the human exosome subunit PM/Scl-100 and are involved in pre-rRNA processing. Nucleic Acids Res *35*, 2564-2572.

Schmidt, M.J., West, S., and Norbury, C.J. (2010). The human cytoplasmic RNA terminal U-transferase ZCCHC11 targets histone mRNAs for degradation. RNA *17*, 39-44.

Shcherbik, N., Wang, M., Lapik, Y.R., Srivastava, L., and Pestov, D.G. (2010). Polyadenylation and degradation of incomplete RNA polymerase I transcripts in mammalian cells. EMBO Rep *11*, 106-111.

Staals, R.H., Bronkhorst, A.W., Schilders, G., Slomovic, S., Schuster, G., Heck, A.J., Raijmakers, R., and Pruijn, G.J. (2010). Dis3-like 1: a novel exoribonuclease associated with the human exosome. EMBO J *29*, 2358-2367.

Stead, J.A., Costello, J.L., Livingstone, M.J., and Mitchell, P. (2007). The PMC2NT domain of the catalytic exosome subunit Rrp6p provides the interface for binding with its cofactor Rrp47p, a nucleic acid-binding protein. Nucleic Acids Res *35*, 5556-5567.

Tomecki, R., Kristiansen, M.S., Lykke-Andersen, S., Chlebowski, A., Larsen, K.M., Szczesny, R.J., Drazkowska, K., Pastula, A., Andersen, J.S., Stepien, P.P.*, et al.*

(2010). The human core exosome interacts with differentially localized processive RNases: hDIS3 and hDIS3L. EMBO J *29*, 2342-2357.

Torchet, C., Bousquet-Antonelli, C., Milligan, L., Thompson, E., Kufel, J., and Tollervey, D. (2002). Processing of 3'-extended read-through transcripts by the exosome can generate functional mRNAs. Mol Cell *9*, 1285-1296.

van Dijk, E.L., Schilders, G., and Pruijn, G.J. (2007). Human cell growth requires a functional cytoplasmic exosome, which is involved in various mRNA decay pathways. RNA *13*, 1027-1035.

van Hoof, A., Lennertz, P., and Parker, R. (2000). Yeast exosome mutants accumulate 3'-extended polyadenylated forms of U4 small nuclear RNA and small nucleolar RNAs. Mol Cell Biol *20*, 441-452.

Vasiljeva, L., and Buratowski, S. (2006). Nrd1 interacts with the nuclear exosome for 3' processing of RNA polymerase II transcripts. Mol Cell *21*, 239-248.

Weir, J.R., Bonneau, F., Hentschel, J., and Conti, E. (2010). Structural analysis reveals the characteristic features of Mtr4, a DExH helicase involved in nuclear RNA processing and surveillance. Proc Natl Acad Sci U S A *107*, 12139-12144.

Wery, M., Ruidant, S., Schillewaert, S., Lepore, N., and Lafontaine, D.L. (2009). The nuclear poly(A) polymerase and Exosome cofactor Trf5 is recruited cotranscriptionally to nucleolar surveillance. RNA *15*, 406-419.

Wilson, M.D., Wang, D., Wagner, R., Breyssens, H., Gertsenstein, M., Lobe, C., Lu, X., Nagy, A., Burke, R.D., Koop, B.F.*, et al.* (2008). ARS2 is a conserved eukaryotic gene essential for early mammalian development. Mol Cell Biol *28*, 1503-1514.

Win, T.Z., Draper, S., Read, R.L., Pearce, J., Norbury, C.J., and Wang, S.W. (2006). Requirement of fission yeast Cid14 in polyadenylation of rRNAs. Mol Cell Biol *26*, 1710-1721.

Wlotzka, W., Kudla, G., Granneman, S., and Tollervey, D. (2011). The nuclear RNA polymerase II surveillance system targets polymerase III transcripts. EMBO J.

Wyers, F., Rougemaille, M., Badis, G., Rousselle, J.C., Dufour, M.E., Boulay, J., Regnault, B., Devaux, F., Namane, A., Seraphin, B.*, et al.* (2005). Cryptic pol II transcripts are degraded by a nuclear quality control pathway involving a new poly(A) polymerase. Cell *121*, 725-737.

Figures 1-7

Click here to download Figure: Figures 1-7 final.pdf

Figure 1

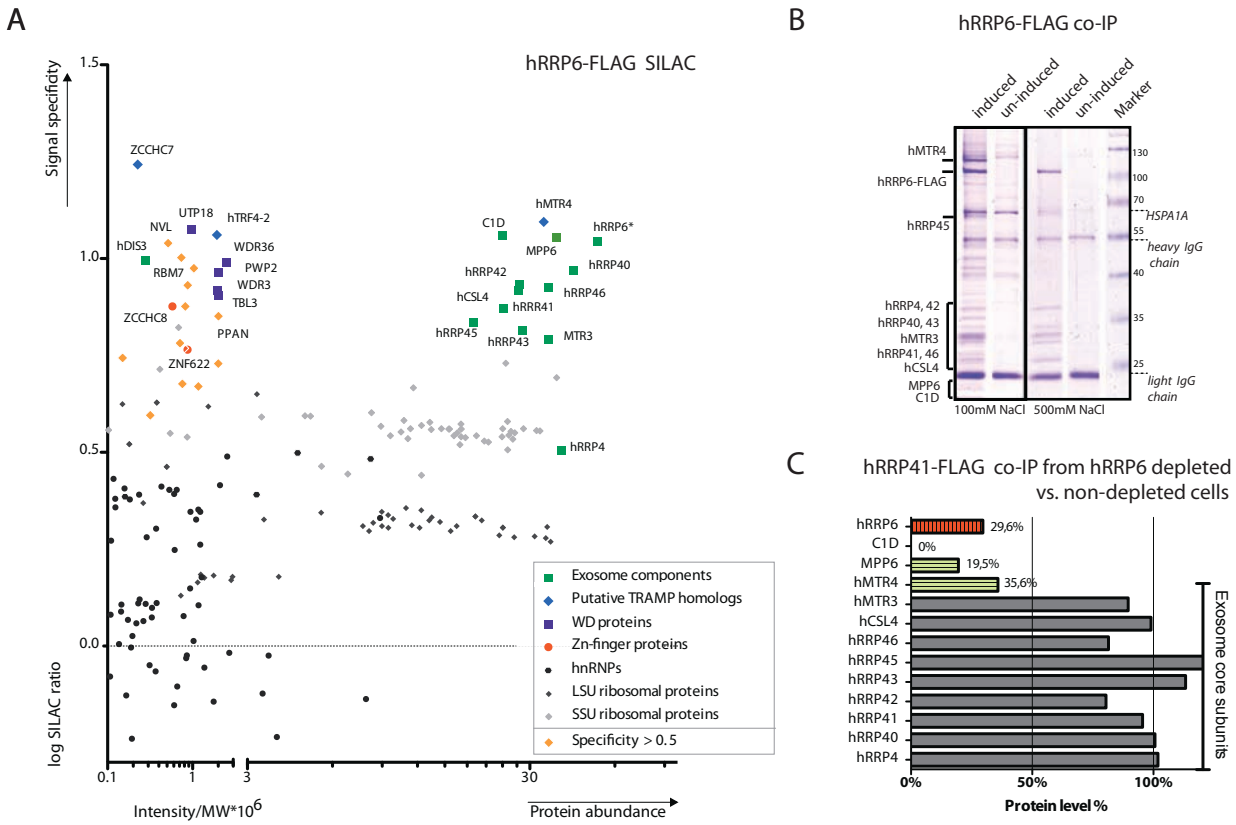

Figure 2

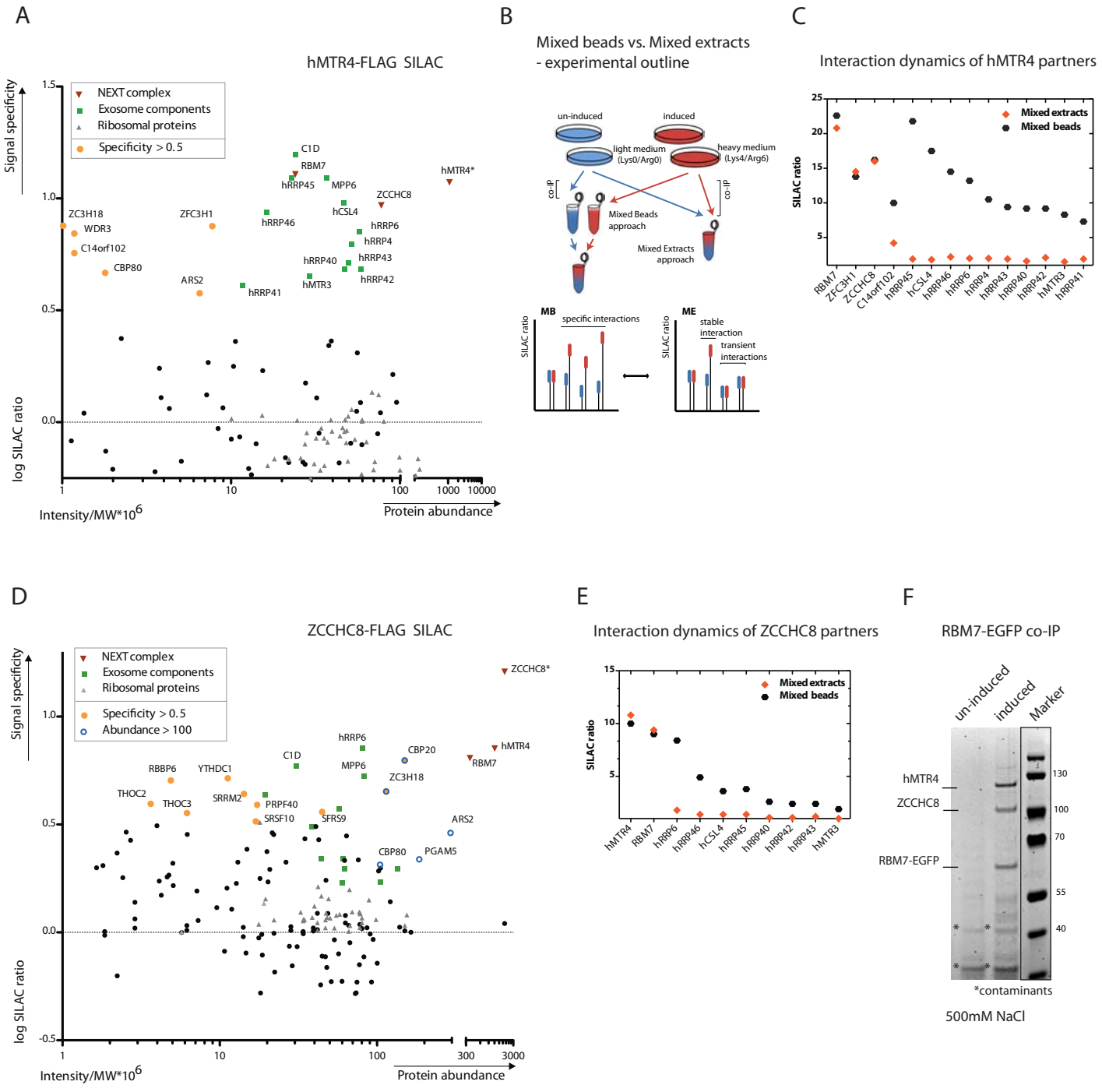
A
hMTR4-FLAG SILAC
NEXT complex
Exosome components
Ribosomal proteins
Specificity > 0.5
Signal specificity
log SILAC ratio
Intensity/MW*10^6
Protein abundance
C1D
RBM7
hRRP45
MPP6
hMTR4*
ZCCHC8
ZC3H18
ZFC3H1
hRRP46
hCSL4
hRRP6
WDR3
hRRP4
C14orf102
hRRP40
hRRP43
CBP80
ARS2
hMTR3
hRRP42
hRRP41
B
Mixed beads vs. Mixed extracts
- experimental outline
un-induced
induced
light medium (Lys0/Arg0)
heavy medium (Lys4/Arg6)
co-IP
Mixed Beads approach
Mixed Extracts approach
MB
specific interactions
ME
stable interaction
transient interactions
SILAC ratio
C
Interaction dynamics of hMTR4 partners
Mixed extracts
Mixed beads
SILAC ratio
RBM7
ZFC3H1
ZCCHC8
C14orf102
hRRP45
hCSL4
hRRP46
hRRP6
hRRP4
hRRP43
hRRP40
hRRP42
hMTR3
hRRP41
D
ZCCHC8-FLAG SILAC
NEXT complex
Exosome components
Ribosomal proteins
Specificity > 0.5
Abundance > 100
Signal specificity
log SILAC ratio
Intensity/MW*10^6
Protein abundance
ZCCHC8*
hRRP6
CBP20
hMTR4
C1D
RBM7
RBBP6
YTHDC1
MPP6
ZC3H18
THOC2
THOC3
SRRM2
PRPF40
SRSF10
SFRS9
ARS2
CBP80
PGAM5
E
Interaction dynamics of ZCCHC8 partners
Mixed extracts
Mixed beads
SILAC ratio
hMTR4
RBM7
hRRP6
hRRP46
hCSL4
hRRP45
hRRP40
hRRP42
hRRP43
hMTR3
F
RBM7-EGFP co-IP
un-induced
induced
Marker
hMTR4
ZCCHC8
RBM7-EGFP
130
100
70
55
40
*contaminants
500mM NaCl

Figure 3

A

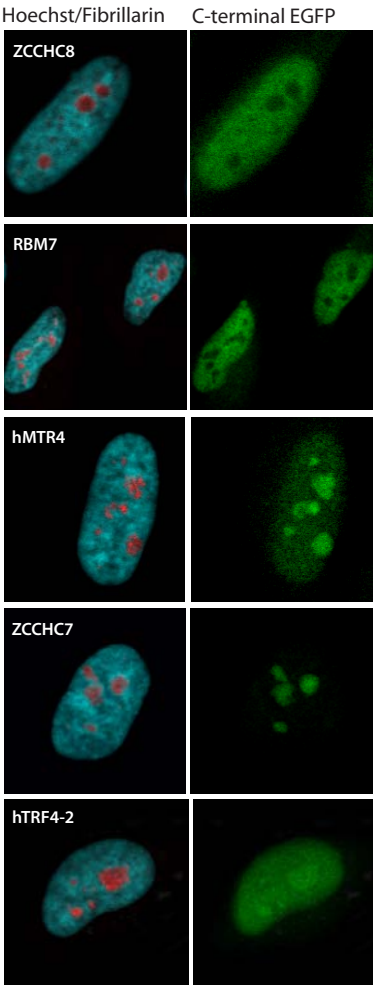

HeLa transiently transfected cells (fixed)

B

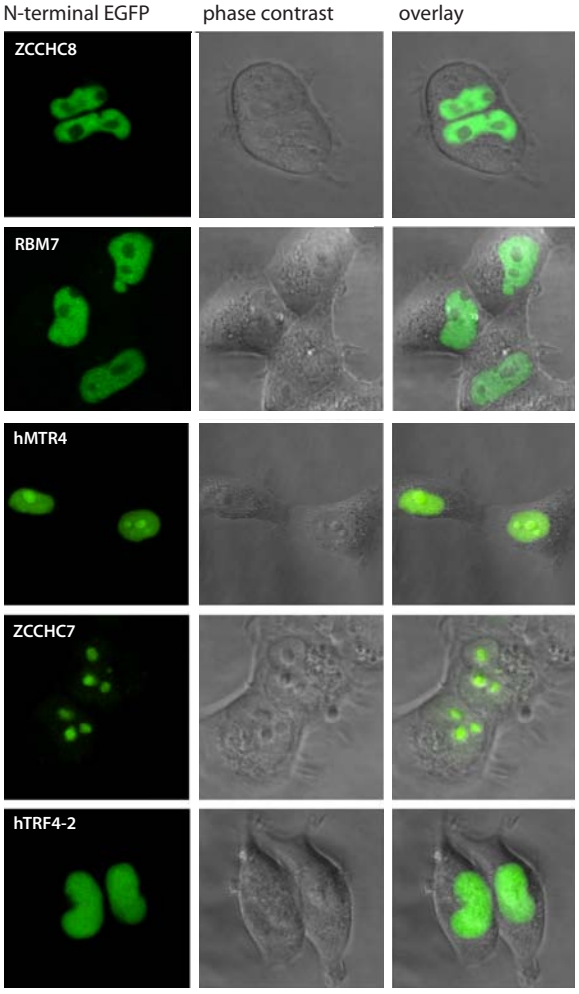

HEK293 stable cells (live imaging)

C

Glycerol gradient analysis

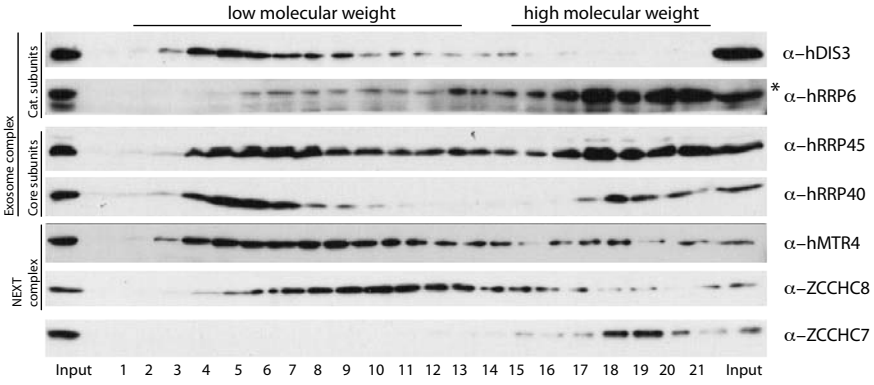

Figure 4

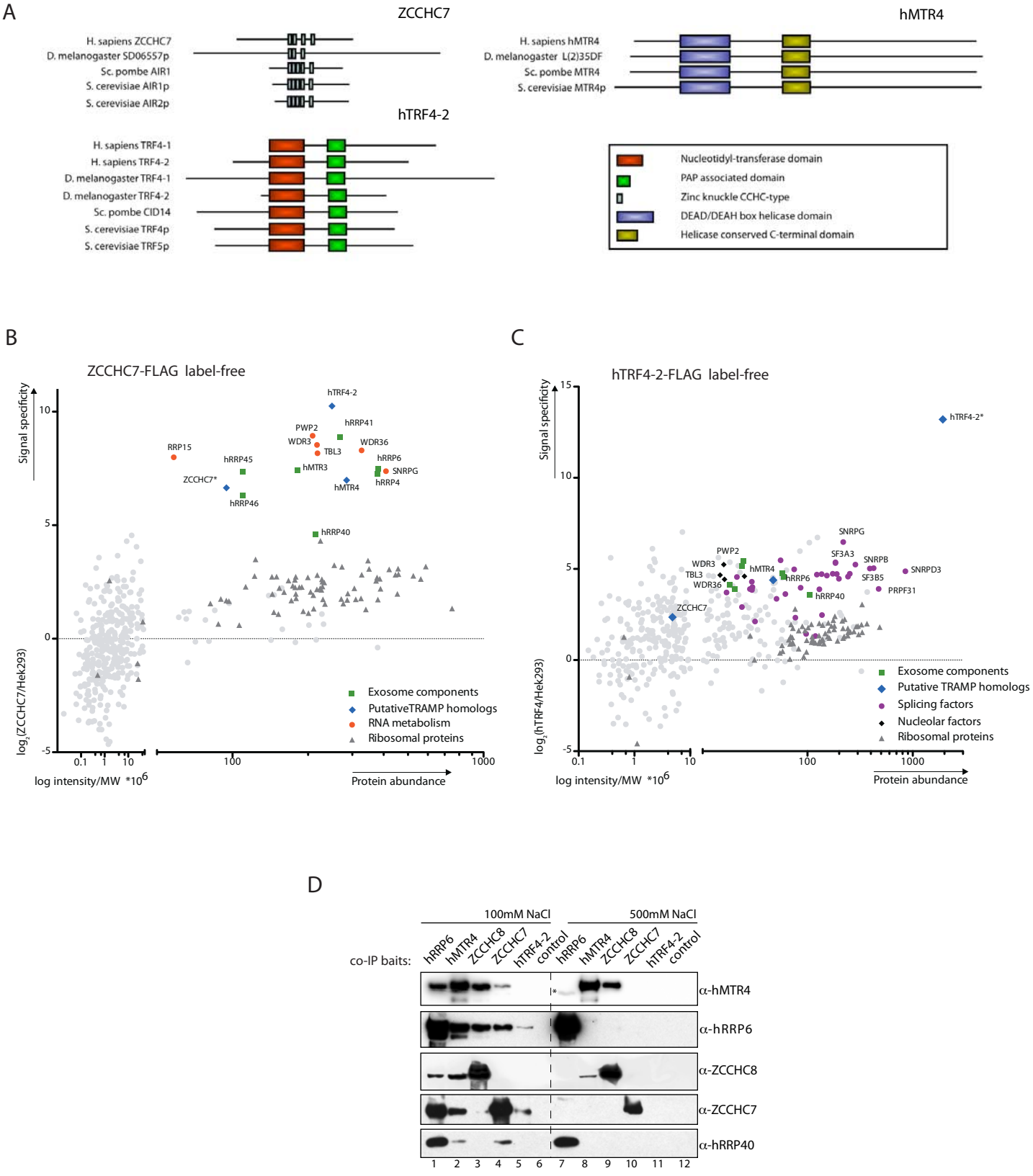
A
ZCCHC7
H. sapiens ZCCHC7
D. melanogaster SD06557p
Sc. pombe AIR1
S. cerevisiae AIR1p
S. cerevisiae AIR2p
hTRF4-2
H. sapiens TRF4-1
H. sapiens TRF4-2
D. melanogaster TRF4-1
D. melanogaster TRF4-2
Sc. pombe CID14
S. cerevisiae TRF4p
S. cerevisiae TRF5p
hMTR4
H. sapiens hMTR4
D. melanogaster L(2)35DF
Sc. pombe MTR4
S. cerevisiae MTR4p
Nucleotidyl-transferase domain
PAP associated domain
Zinc knuckle CCHC-type
DEAD/DEAH box helicase domain
Helicase conserved C-terminal domain
B
ZCCHC7-FLAG label-free
Signal specficity
log2(ZCCHC7/Hek293)
log intensity/MW *10^6
Protein abundance
hTRF4-2
hRRP41
PWP2
WDR3
WDR36
TBL3
RRP15
hRRP45
hRRP6
hMTR3
SNRPG
ZCCHC7*
hRRP4
hMTR4
hRRP46
hRRP40
Exosome components
PutativeTRAMP homologs
RNA metabolism
Ribosomal proteins
C
hTRF4-2-FLAG label-free
Signal specificity
log2(hTRF4/Hek293)
log intensity/MW *10^6
Protein abundance
hTRF4-2*
SNRPG
PWP2
SF3A3
SNRPB
SNRPD3
WDR3
hMTR4
TBL3
hRRP6
SF3B5
WDR36
PRPF31
hRRP40
ZCCHC7
Exosome components
Putative TRAMP homologs
Splicing factors
Nucleolar factors
Ribosomal proteins
D
100mM NaCl
500mM NaCl
co-IP baits:
hRRP6
hMTR4
ZCCHC8
ZCCHC7
hTRF4-2
control
α-hMTR4
α-hRRP6
α-ZCCHC8
α-ZCCHC7
α-hRRP40
1 2 3 4 5 6 7 8 9 10 11 12

Figure 5

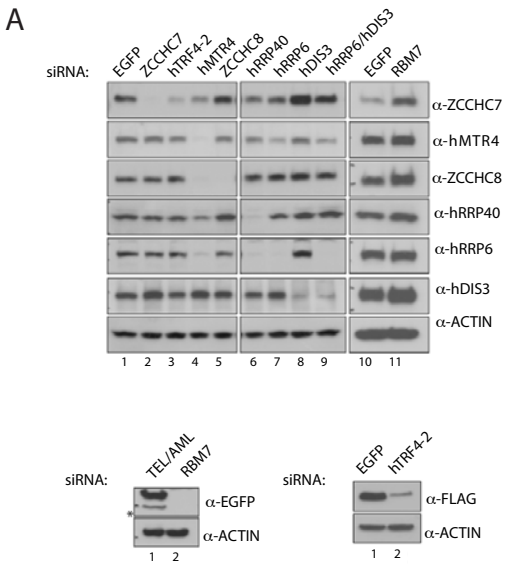
A
siRNA:
EGFP
ZCCHC7
hTRF4-2
hMTR4
ZCCHC8
hRRP40
hRRP6
hDIS3
hRRP6/hDIS3
EGFP
RBM7
α-ZCCHC7
α-hMTR4
α-ZCCHC8
α-hRRP40
α-hRRP6
α-hDIS3
α-ACTIN
1 2 3 4 5 6 7 8 9 10 11
siRNA:
TEL/AML
RBM7
α-EGFP
α-ACTIN
1 2
siRNA:
EGFP
hTRF4-2
α-FLAG
α-ACTIN
1 2

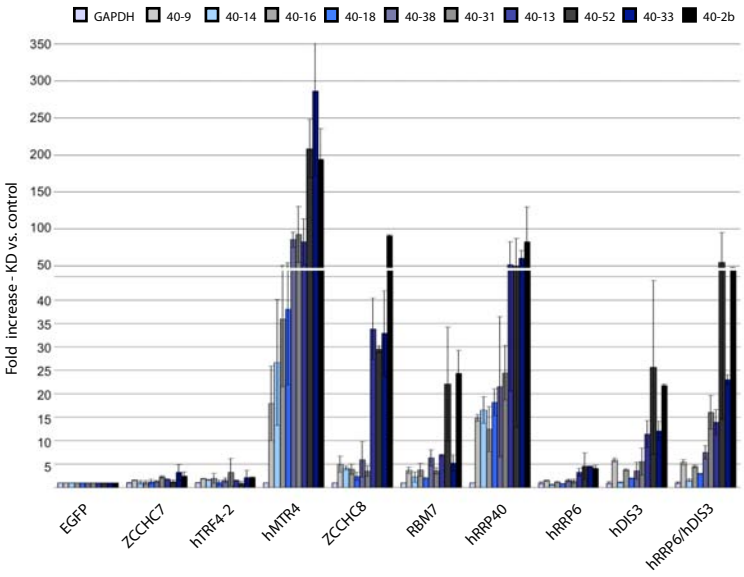
B
GAPDH
40-9
40-14
40-16
40-18
40-38
40-31
40-13
40-52
40-33
40-2b
Fold increase - KD vs. control
350
300
250
200
150
100
50
40
35
30
25
20
15
10
5
EGFP
ZCCHC7
hTRF4-2
hMTR4
ZCCHC8
RBM7
hRRP40
hRRP6
hDIS3
hRRP6/hDIS3

Figure 6

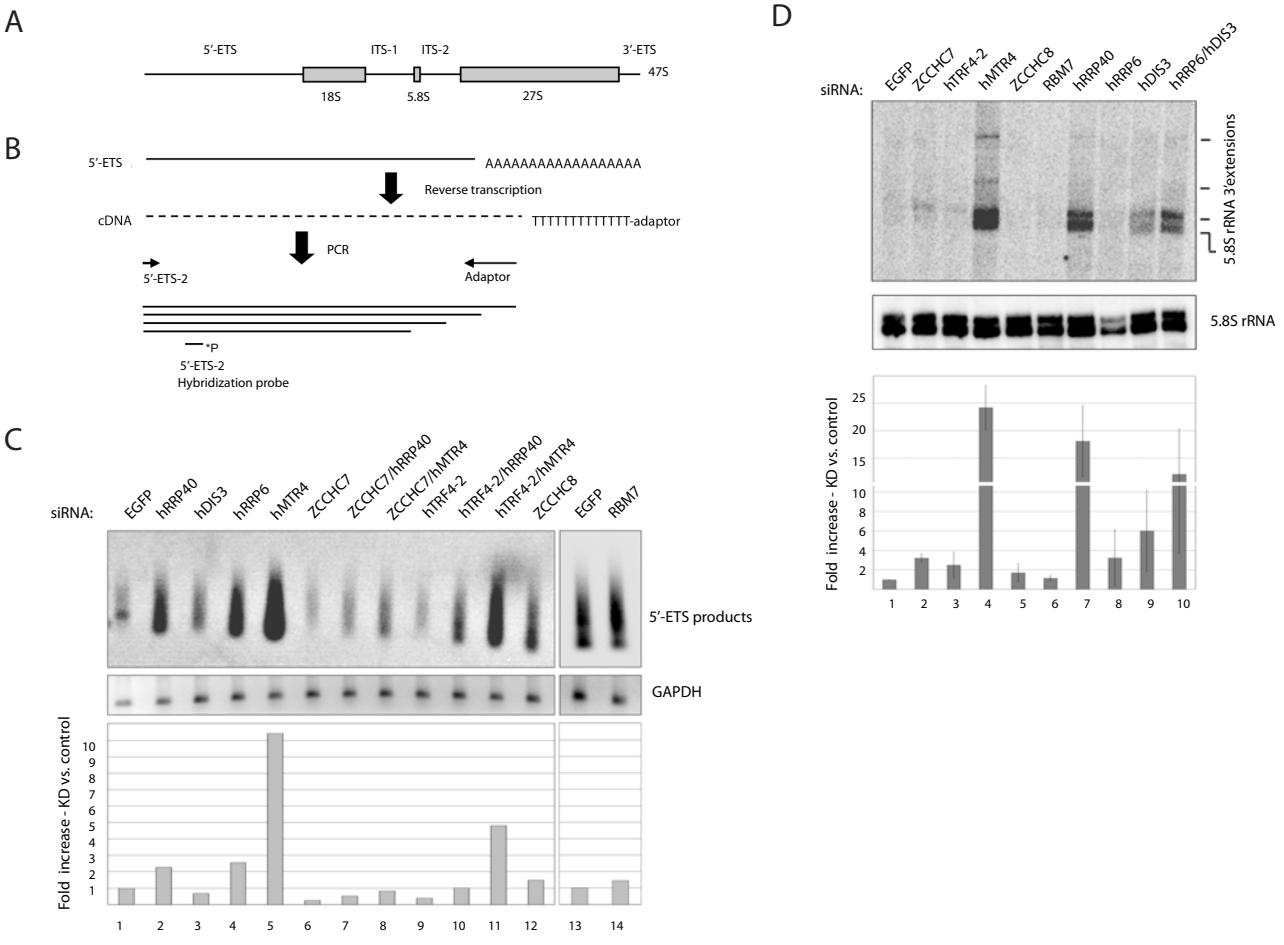
A
5′-ETS
ITS-1
ITS-2
3′-ETS
47S
18S
5.8S
27S
B
5′-ETS
AAAAAAAAAAAAAAAAA
Reverse transcription
cDNA
TTTTTTTTTTTT-adaptor
PCR
5′-ETS-2
Adaptor
*P
5′-ETS-2
Hybridization probe
C
siRNA:
EGFP
hRRP40
hDIS3
hRRP6
hMTR4
ZCCHC7
ZCCHC7/hRRP40
ZCCHC7/hMTR4
hTRF4-2
hTRF4-2/hRRP40
hTRF4-2/hMTR4
ZCCHC8
EGFP
RBM7
5′-ETS products
GAPDH
Fold increase - KD vs. control
1 2 3 4 5 6 7 8 9 10 11 12 13 14
D
siRNA:
EGFP
ZCCHC7
hTRF4-2
hMTR4
ZCCHC8
RBM7
hRRP40
hRRP6
hDIS3
hRRP6/hDIS3
5.8S rRNA 3′extensions
5.8S rRNA
Fold increase - KD vs. control
1 2 3 4 5 6 7 8 9 10

Figure 7

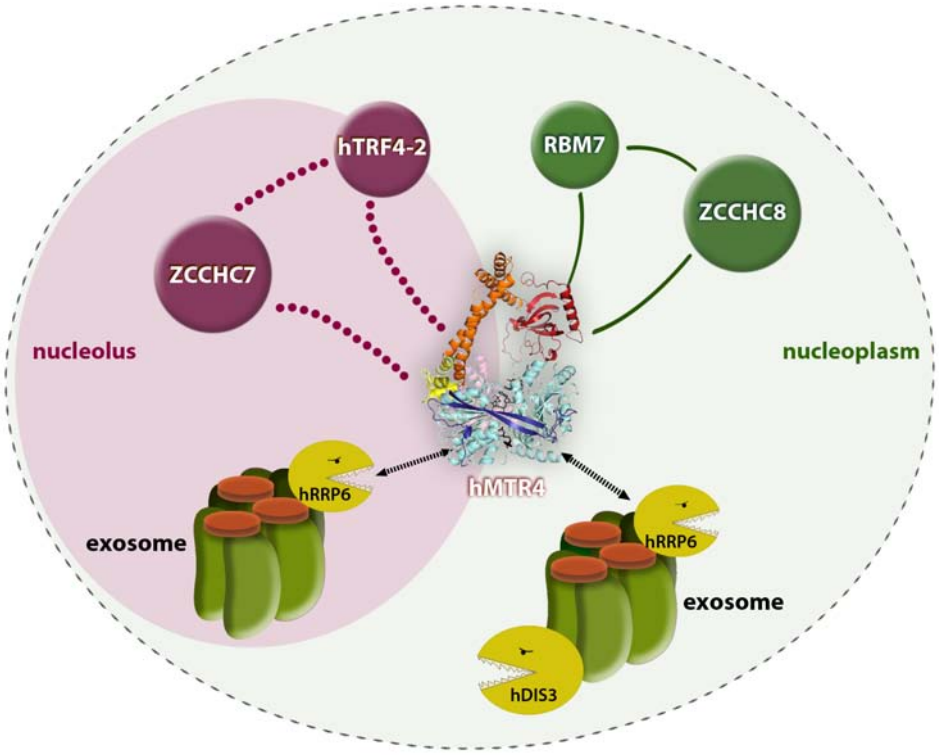
hTRF4-2
RBM7
ZCCHC8
ZCCHC7
nucleolus
nucleoplasm
hMTR4
hRRP6
exosome
hRRP6
exosome
hDIS3

Supplemental Figures 1-4

Click here to download Supplemental Figure: Figures S1-S4 final.pdf

Figure S1

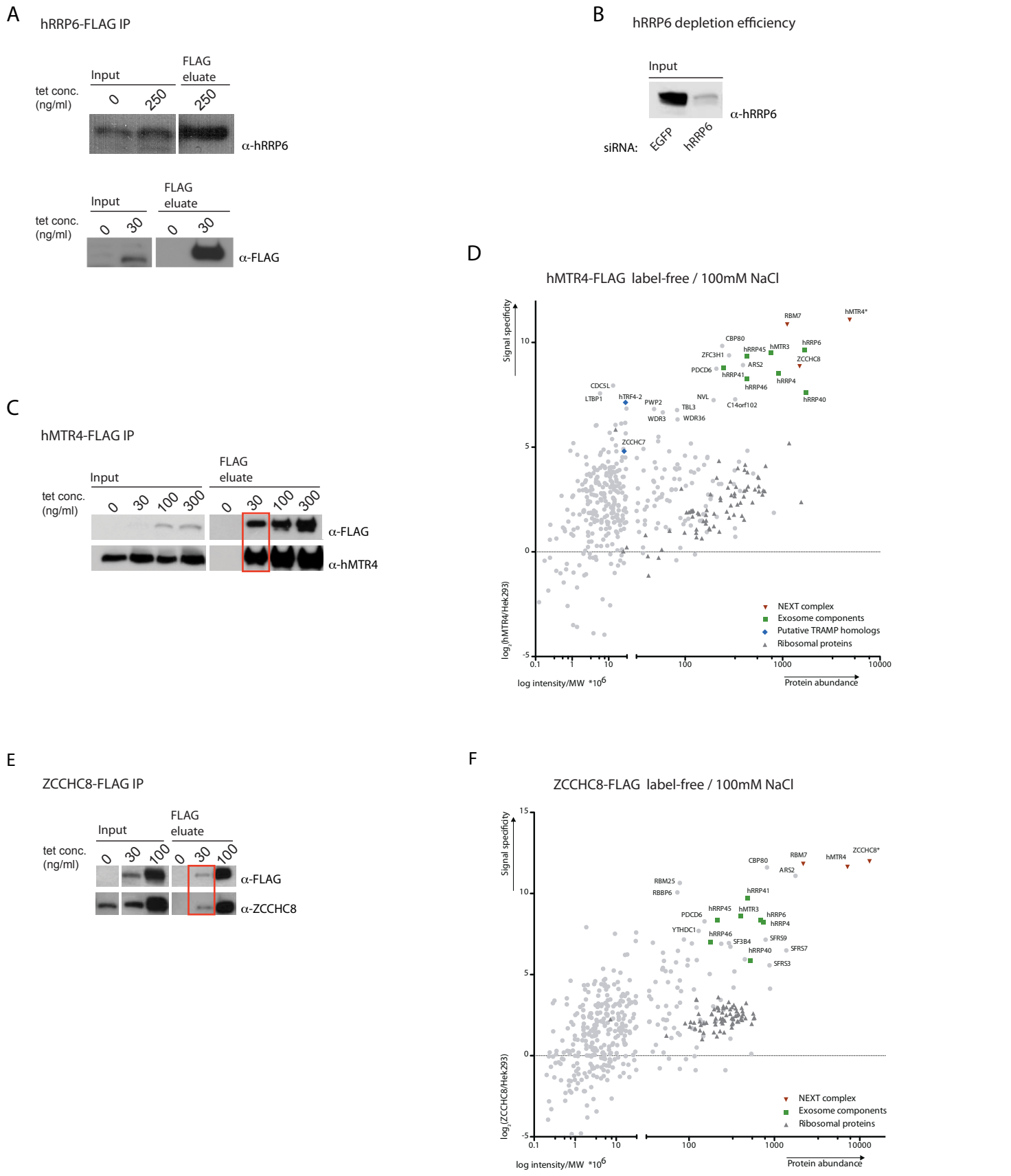

Figure S2

A

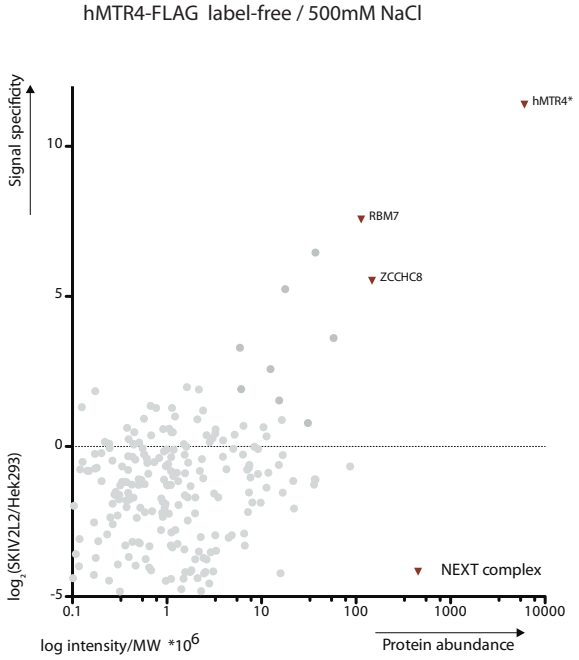
hMTR4-FLAG label-free / 500mM NaCl
Signal specificity
log2(SKIV2L2/Hek293)
hMTR4*
RBM7
ZCCHC8
NEXT complex
log intensity/MW *10^6
Protein abundance

B

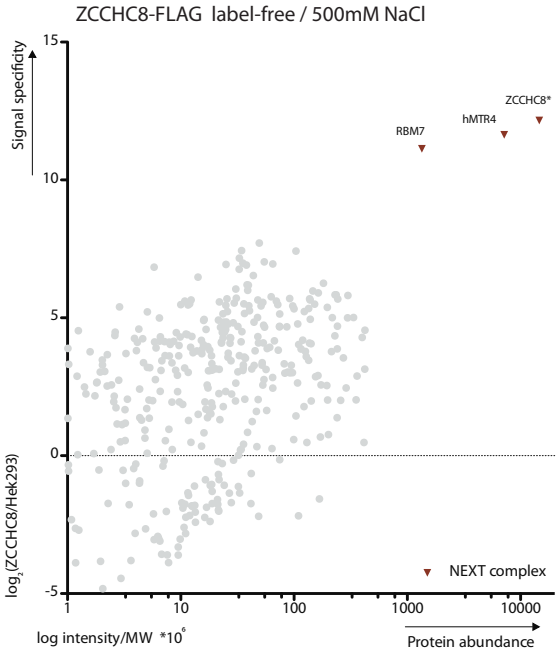
ZCCHC8-FLAG label-free / 500mM NaCl
Signal specificity
log2(ZCCHC8/Hek293)
ZCCHC8*
hMTR4
RBM7
NEXT complex
log intensity/MW *10^6
Protein abundance

Figure S3

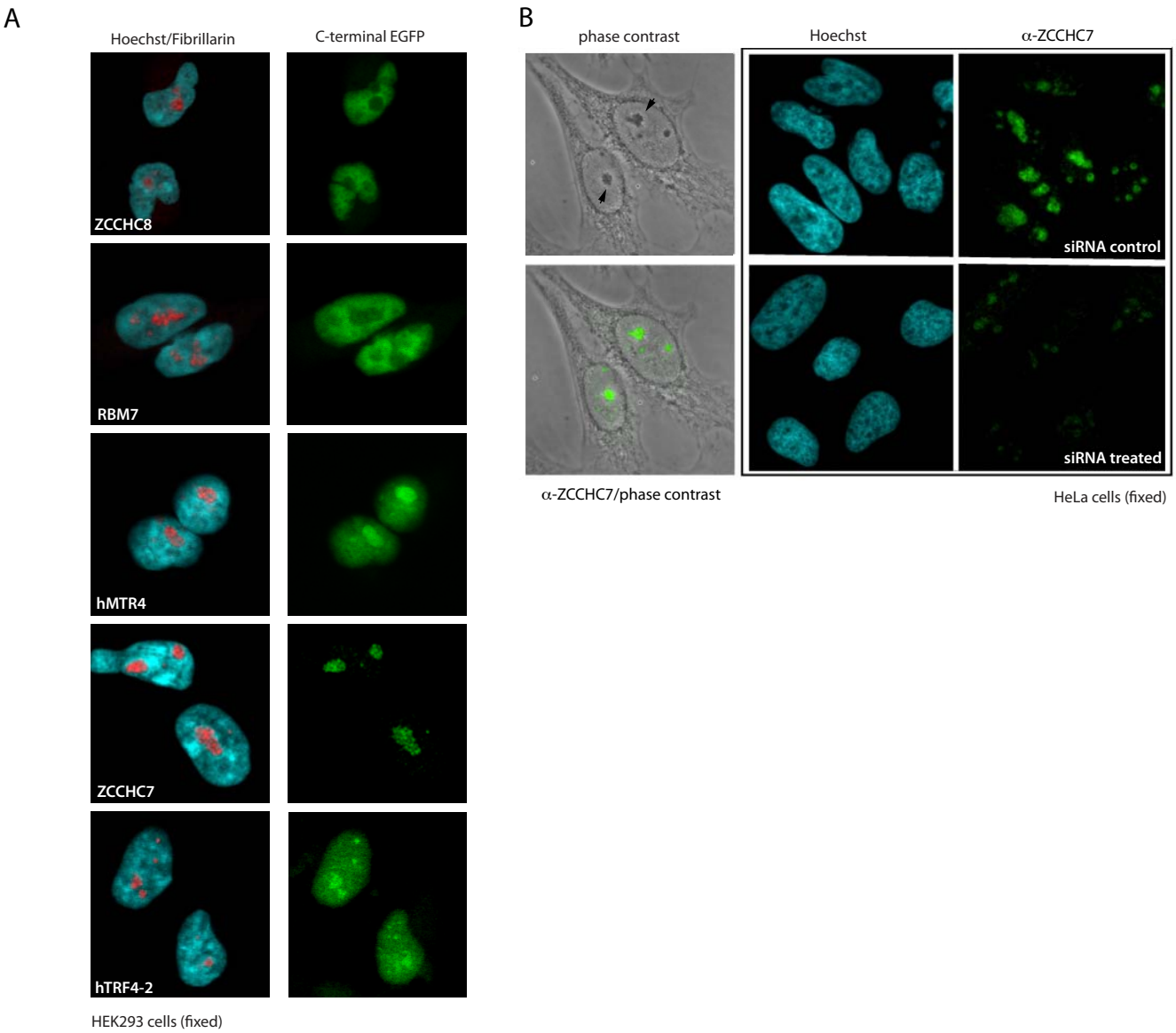
A
Hoechst/Fibrillarin
C-terminal EGFP
ZCCHC8
RBM7
hMTR4
ZCCHC7
hTRF4-2
HEK293 cells (fixed)
B
phase contrast
Hoechst
α-ZCCHC7
siRNA control
siRNA treated
α-ZCCHC7/phase contrast
HeLa cells (fixed)

Figure S4

A

Sequence alignment of ZCCHC7 with its closest homologs

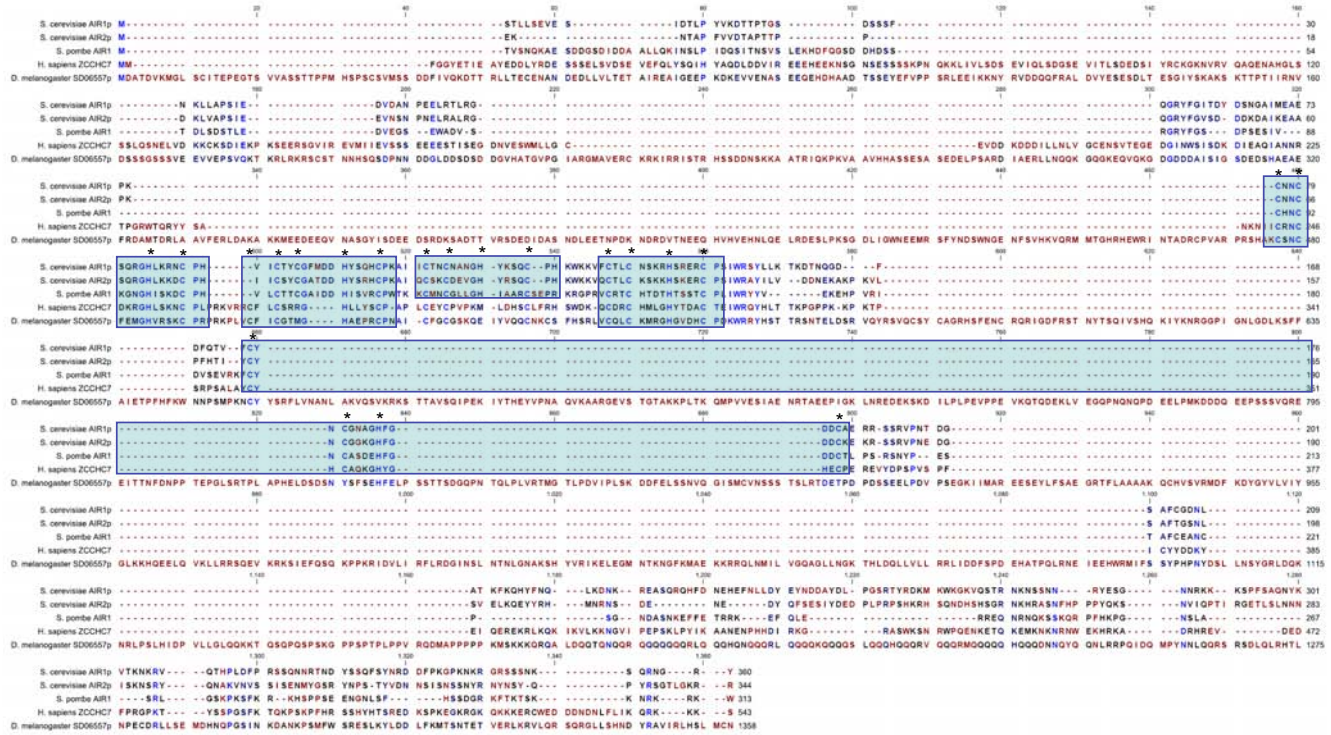

B

Sequence alignment of hTRF4-2 with its closest homologs

Figure S4

C

Sequence alignment of hMTR4 (SKIV2L2) with its closest homologs.

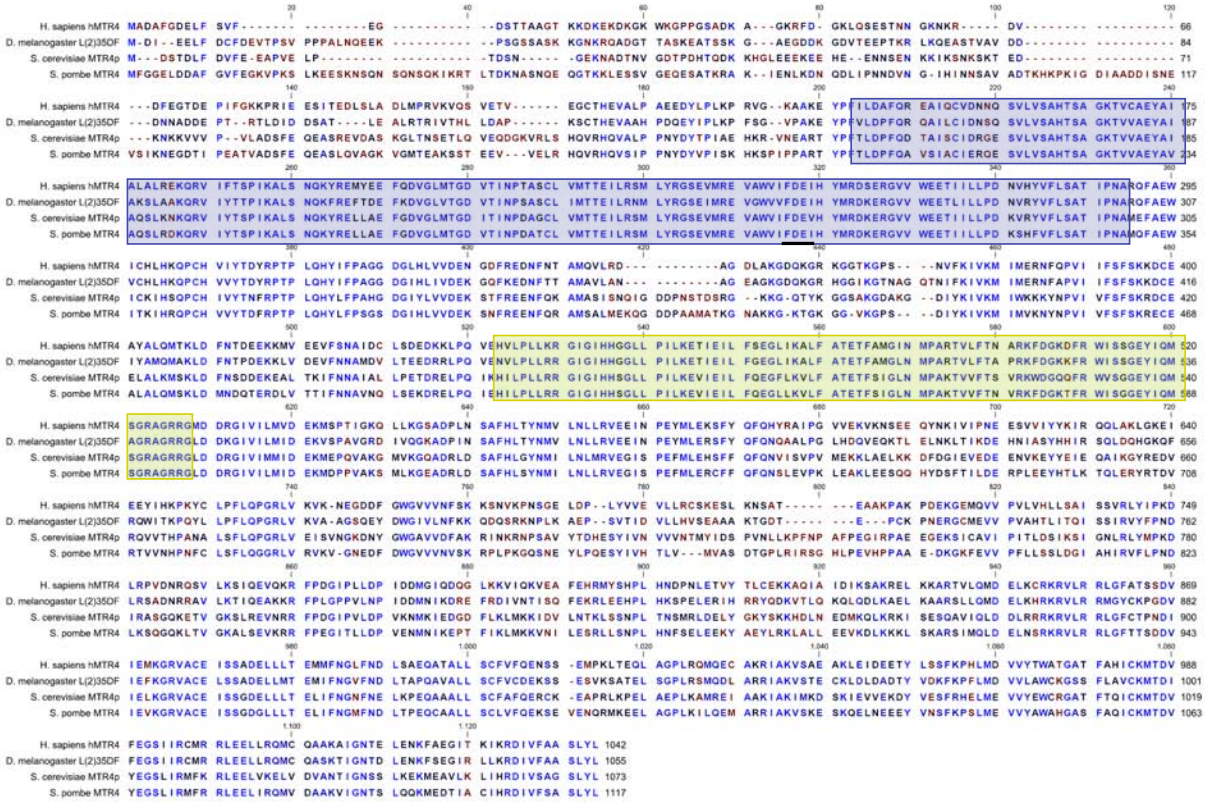

D

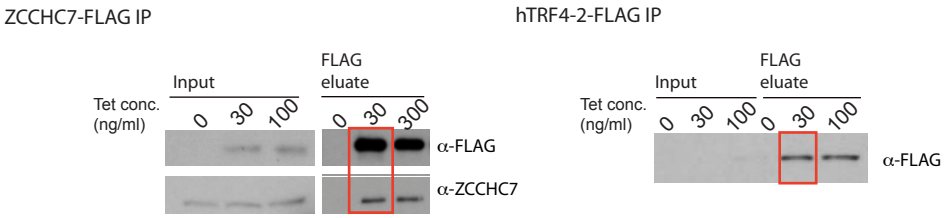

Supplemental Tables 1-14

Click here to download Supplemental Movies and Spreadsheets: Tables S1-S14 final.pdf